STM JOURNALS

International Journal of
Energy and Thermal Applications

ISSN: 3108-1479
Volume 4, Issue 2, 2026
July–December
DOI (Journal): 10.37591/IJETA

https://journals.stmjournals.com/ijeta

Research IJETA

Study of Technical and Economic Assessment of Solar-Assisted and Thermoelectric Air-Conditioning Technologies

Nagendra Singh[1,*], Sanjeev Kumar Verma[2], Manish Dixit[3]

Abstract

This study presents an integrated technical and economic assessment of solar-assisted absorption and thermoelectric air-conditioning technologies for residential cooling applications. A comprehensive methodology combining mathematical modeling, experimental characterization of thermoelectric modules, numerical simulation, and economic optimization was developed to evaluate the performance of both cooling systems. The solar-assisted system employs single-effect LiBr–H_2O absorption chillers operating under water-cooled and air-cooled configurations, simulated using transient system simulation tool (TRNSYS) and the Engineering Equation Solver (EES), while the thermoelectric air-conditioning system was analyzed using experimentally determined module characteristics. The proposed economic optimization is based on the economic total cooling capacity (ETCC), which simultaneously considers cooling performance, investment cost, and operating cost. The results indicate that the optimum water-cooled solar absorption system requires an 18 m² evacuated tube collector field and a 1.26 m³ thermal storage tank, providing approximately 55% of the annual cooling energy demand, whereas the air-cooled configuration requires a 16 m² collector area and a 0.98 m³ storage tank with nearly 45% solar energy contribution. For the thermoelectric system, the optimized operating conditions improve the balance between cooling capacity and lifecycle cost, demonstrating that maximum economic performance is achieved below the maximum cooling capacity and that the system can be overloaded by approximately 32% under reference conditions without significant economic penalty. The novelty of this work lies in the development of a unified technical-economic framework integrating solar-assisted absorption cooling and thermoelectric air-conditioning with experimental validation and ETCC-based optimization. The proposed methodology provides practical design guidelines for developing energy-efficient, environmentally friendly, and economically viable residential air-conditioning systems while reducing electricity consumption and dependence on conventional refrigerants.

Keywords: Single-effect chiller, evacuated tube collectors, solar air-conditioning, economic viability, thermoelectric cooler, economic analysis, thermal resistance

***Author for Correspondence**
Nagendra Singh
E-mail: singh.mech2008@gmail.com

[1,3]Assistant Professor, Department of Mechanical Engineering, Institute of Engineering and Technology, Dr. Bhimrao Ambedkar University, Swami Vivekanand Campus, Khandari, Agra, Uttar Pradesh, India
[2]Assistant Professor Department of Mechanical Engineering, Central Instrumentation Facility Research and Development Cell, Lovely Professional University, Phagwara, Punjab, India

Received Date: June 10, 2026
Accepted Date: July 06, 2026
Published Date: July 23, 2026

Citation: Nagendra Singh, Sanjeev Kumar Verma, Manish Dixit. Study of Technical and Economic Assessment of Solar-Assisted and Thermoelectric Air-Conditioning Technologies. International Journal of Energy and Thermal Applications. 2026; 4(2): 36–64p.

INTRODUCTION

Over the past few decades, the use of electricity-driven air-conditioning units has surged, causing a sharp rise in fossil fuel consumption and, in many countries, especially in hot regions, frequent grid overloads during summer peak demand. In 1996, small air conditioners (up to 12 kW cooling capacity) consumed roughly 11,000 GWh of primary energy; this figure was projected to quadruple by 2020. At the same time, particularly over the last ten years, extensive research has focused on reducing or eliminating environmentally harmful refrigerants and

© STM Journals 2026. All Rights Reserved

developing technologies that lower the electrical energy required for cooling [1]. This trend has created a market for thermally driven chillers. A key benefit is that peak seasonal cooling demand aligns with periods of high solar radiation. The first solar-assisted absorption chiller was demonstrated using the technique developed by Edmond Carré. Two main factors explain the growing interest: worsening environmental impacts from fossil fuel electricity used by conventional compression chillers, and the substantially improved conditions for adopting solar technology compared with earlier times. For solar-assisted air-conditioning using conventional collectors (flat-plate and evacuated tube), single-effect absorption chillers cooled by either air or water are the most appropriate option because they operate with relatively low-temperature heat input while delivering reasonable performance, with COPs typically between 0.7 and 0.9. Chillers that use aqueous lithium bromide (LiBr) solutions are commercially available at low capacities, beginning around 4 kW, making them suitable for a range of buildings from single-family homes to large commercial facilities. The selection of the LiBr/water working pair is justified by the following reasons [2]. For the single-effect chiller considered here, driver fluid temperatures only slightly above 105°C, which evacuated tube collectors can provide, are adequate. Prior studies have also shown that LiBr/water machines outperform water/ammonia systems. Moreover, since air-conditioning does not require evaporation temperatures below 5°C, water can be used as a refrigerant. This study examines the technical and economic viability of a solar-driven air-conditioning system through mathematical modeling and numerical simulation. Simulations were carried out with TRNSYS for solar applications and the general-purpose algebraic solver EES. Two single-effect LiBr–H_2O absorption chillers, cooled either by air or by water, were sized for a typical middle-class home (175 m²) under the given climate [3]. The solar-assisted system includes the chiller, a field of evacuated tube collectors, a gas-fired auxiliary heater, a hot water storage tank, and fan-coil units for space conditioning.

In many parts of the world, ambient temperatures often rise well above comfortable levels, making room air-conditioning necessary for comfortable living and working environments. Maintaining indoor temperatures within the thermal comfort range improves well-being and productivity. Climate control is also critical in heavy machinery and transport, where personnel may be exposed to extreme conditions for extended periods. For occupant comfort, systems should be compact, portable, and quiet, attributes that thermoelectric coolers (TECs) can provide. The electric vehicle industry has similar requirements [4]. Relevant reports show that in many countries, household spending on room air-conditioning represents a substantial portion of electricity bills. Air conditioners also significantly affect global warming. Climate impacts arise not only from the electricity consumed for cooling but also from refrigerants like chlorofluorocarbons (CFCs) and hydrochlorofluorocarbons (HCFCs), which amplify the greenhouse effect. The study finds that energy use is higher in cities and is influenced more by the number of households than by the total population. This has prompted organizations, including the United Nations, to pursue measures to curb electricity consumption. Concurrently, research aims to quantify cooling demand and optimize its use, particularly by incorporating comfort metrics. Advanced control strategies and algorithms can improve cooling efficiency, and these gains apply to both stationary systems and passenger vehicles.

Conventional room-cooling systems, whether portable or wall-mounted, primarily rely on compressor-based air conditioners operating on the refrigeration cycle. Thermoelectric modules offer a potential alternative to these traditional systems. In a thermoelectric module powered by electricity, a temperature gradient is produced by absorbing heat through the Peltier effect at one junction and releasing it at the opposite junction. These modules generally consist of two dissimilar materials possessing suitable thermoelectric properties, connected electrically in a series–parallel arrangement while remaining thermally connected in parallel [5]. The module structure comprises legs made from two different materials, positioned between ceramic plates that serve as the outer covering. The use of thermoelectric devices in zero-emission buildings, particularly for air-conditioning applications, has attracted considerable attention. An experimental investigation of a solar-powered thermoelectric air-conditioning system integrated with hot water production has been reported. The results demonstrated a relatively high coefficient of performance (COP) when simultaneously providing space cooling and

© STM Journals 2026. All Rights Reserved

water heating. Dongxu et al. addressed the simulation and optimization of the internal configuration of thermoelectric elements used in air-conditioning systems. A comparable study focusing on transient operating conditions has also been presented in the literature. Studies have been reported on systems that integrate thermoelectric modules into ceilings in conjunction with room ventilation and airflow management, as well as systems that combine thermoelectric technology with solar energy sources. Yilmazoglu conducted experimental investigations on a prototype thermoelectric heating, ventilation, and air conditioning (HVAC) system comprising a thermoelectric module and heat radiators installed within ventilation ducts. The experimental setup employed a single TEC, and observations were made regarding the airflow characteristics and thermal performance of the system.

The internal configuration of thermoelectric modules can be further enhanced through optimization, including the adoption of unconventional leg geometries. Several innovative non-planar thermoelectric module designs have been reported in the literature [6]. The authors of another study investigated multistage refrigeration systems employing TECs. Attar and Lee proposed a thermoelectric air-conditioning system incorporating air-to-air heat exchangers for automotive applications and optimized its performance by varying the electric current and number of thermoelectric modules. Sun et al. introduced a novel radiant heating terminal integrated with a TEC and evaluated its performance under actual operating conditions. The proposed system was found to operate more efficiently and achieve the desired conditions more rapidly than conventional systems. Significant progress is currently being made in the development of advanced thermoelectric materials, which is expected to lead to the availability of more efficient thermoelectric modules in the future. A comprehensive review of thermoelectric modules and their diverse applications has been presented in the literature. The heat absorbed by a thermoelectric module must be removed from the conditioned space and dissipated to the surrounding environment. This process is commonly accomplished using finned radiators assisted by fans, sometimes with the aid of a liquid coolant that transfers heat between the TEC and the radiator. Effective heat removal can only be achieved when the radiators possess sufficient heat transfer capacity. The heat transfer medium may be either liquid water or a phase-change material (PCM) that utilizes latent heat during phase transitions [7]. The selection of an air-conditioning system for a particular application should not be based solely on the COP of the unit and the cooling load required to maintain a specified temperature. It is also essential to consider the system's operational behavior, energy consumption over a complete 24-h period, and the associated investment costs. A key aspect of such analyses is the determination of peak power demand while accounting for the thermal storage capacity and dynamic thermal response of the building. In integrated systems incorporating multiple chillers, the control strategies used to regulate each unit and achieve optimal operating conditions can be highly advanced and complex. To improve energy efficiency, the heat rejected by the air-conditioning condenser (outdoor heat exchanger) can be recovered and utilized for applications such as domestic water heating instead of being discharged into the environment. The concept of partial energy recovery from air-conditioning systems, along with indoor humidity regulation, has been discussed in the literature [8]. Luqman and Al-Ansari also proposed an innovative approach for using air-conditioning systems to generate clean water. Notably, this technique can be implemented irrespective of the specific type of air-conditioning system employed.

Most air-conditioning systems currently in use operate through compressors powered by mechanical energy, which is typically supplied by an electric motor. This principle applies to vehicle air-conditioning units, large-scale industrial cooling systems, and domestic air-conditioning appliances. The present study focuses on smaller air-conditioning units designed for residential applications, with particular attention given to portable air conditioners that are housed entirely within a single self-contained enclosure. A major challenge associated with these devices is the removal of heat from the conditioned space to the external environment. This is commonly accomplished by expelling heated air outside the room through an attached exhaust duct, often in the form of a flexible corrugated hose. Furthermore, these air conditioners often produce relatively high noise levels during operation, while also being bulky and heavy owing to their large housing [9]. Many of the drawbacks associated with conventional compressor-based air-conditioning systems can be addressed through the use of

© STM Journals 2026. All Rights Reserved

thermoelectric technology. Thermoelectric systems can be effectively employed in buildings, heavy equipment such as cranes, and electric vehicles for applications including cabin climate regulation and seat cooling. They are also well suited for situations requiring accurate temperature control. In addition to their versatility, thermoelectric systems feature a simple design and operate without the need for environmentally harmful refrigerants, making them an attractive alternative to traditional cooling technologies. In addition, the system can be easily and continuously regulated by adjusting the supplied electric current. This study proposes a thermoelectric air-conditioning system in which a group of thermoelectric modules functions as a heat pump. Heat is extracted from the conditioned space and rejected to the surrounding environment through an environmentally benign working fluid, such as water, in combination with heat exchangers located on both sides of the system. The performance of the proposed configuration was evaluated from both technical and economic perspectives, and the system design was optimized to maximize the overall economic viability of the solution. Since the COP reflects only the efficiency of the system, a new metric termed Economic Total Cooling Capacity (ETCC) was introduced to account for both investment and operating costs over a specified period [10]. The analysis was carried out using commercially available thermoelectric modules, whose performance characteristics were determined through experimental measurements. To the best of the authors' knowledge, such a comprehensive evaluation has not been reported previously. The findings provide valuable insight into the feasibility and economic justification of developing and operating the proposed TEC-based air-conditioning system.

Limitations of Existing Technologies and Scope of the Present Work

Conventional vapor-compression air-conditioning systems are widely used because of their high cooling capacity and mature technology; however, they suffer from high electricity consumption, dependence on fossil fuel-based power generation, peak-load demand on electrical grids, and the use of refrigerants with significant environmental impacts. Solar-assisted absorption cooling systems offer a sustainable alternative but are constrained by their high initial investment, dependence on solar radiation availability, large collector and thermal storage requirements, and relatively low economic feasibility for small residential applications. Similarly, thermoelectric cooling systems provide advantages such as compact size, silent operation, precise temperature control, scalability, and the absence of environmentally harmful refrigerants; however, their relatively low COP, limited cooling capacity, high material cost, and sensitivity to heat exchanger performance restrict their widespread application. Moreover, most previous studies have focused either on the technical performance or on the economic aspects of these technologies individually, while comprehensive optimization considering both technical and economic criteria remains limited. To address these shortcomings, the present study develops an integrated technical-economic assessment framework for solar-assisted absorption and thermoelectric air-conditioning systems, incorporating mathematical modeling, experimental validation of thermoelectric module characteristics, numerical simulation, and economic optimization using the ETCC criterion. This approach enables the selection of optimal system configurations that simultaneously improve energy efficiency and economic viability for residential cooling applications.

Limitations of the Present Work

Although the proposed methodology provides a comprehensive technical and economic assessment of solar-assisted and thermoelectric air-conditioning systems, several limitations remain. The analysis is based on numerical simulations supported by the experimental characterization of commercially available thermoelectric modules rather than a full-scale integrated prototype. The solar-assisted system was evaluated under specific climatic conditions and residential building configurations, which may influence its applicability to other geographical regions or building types. Economic analysis was performed using assumed market prices, electricity tariffs, and operating conditions that may vary over time and across locations. In addition, the study considered steady-state operating conditions for most simulations and did not include long-term degradation of thermoelectric modules, collector performance, maintenance uncertainties, or dynamic control strategies. Future research should include large-scale experimental validation, multi-climate analysis, life cycle assessment, and intelligent control algorithms to further improve the practical applicability and reliability of the proposed system.

© STM Journals 2026. All Rights Reserved

Table 1. Comparative analysis of the proposed work with previous studies.

References	Reported work	Major focus	Limitations of existing work	Advantages of the proposed study
Mao et al. [1]	Building energy-saving air-conditioning system	Building thermal comfort and energy efficiency	Focused only on building energy performance; no economic optimization or renewable integration	Integrates renewable solar cooling with detailed technical and economic optimization.
Mei and Xia [2, 10]	Predictive and hierarchical control of air-conditioning systems	Control strategy for energy-efficient cooling	Limited to conventional vapor-compression systems; no thermoelectric or solar-assisted analysis	Develops an integrated solar-assisted and thermoelectric cooling framework with economic assessment.
Liu et al. [11, 12]	Solar thermoelectric air-conditioning system	Experimental evaluation of solar-powered TEC cooling	No comprehensive economic optimization or residential system design	Includes experimental validation together with lifecycle economic optimization (ETCC).
Dongxu et al. [13]	Geometry optimization of thermoelectric modules	Optimization of TEC internal geometry	Limited to module-level optimization; system-level analysis absent	Optimizes the complete air-conditioning system including modules, radiators, operating current, and cost.
Attar and Lee [14]	Automotive thermoelectric air-conditioner	Design optimization for vehicle cooling	Applicable only to automotive applications; no solar integration	Extends thermoelectric optimization to residential cooling and combines it with solar-assisted absorption technology.
Martinez et al. [15, 16]	Thermoelectric heat pumps for nearly zero energy buildings	Simulation of thermoelectric heat pumps	Focuses mainly on thermal performance; economic evaluation not included	Simultaneously evaluates technical performance, experimental validation, and economic feasibility.
Provensi and Barbosa [17]	Multistage thermoelectric cooling optimization	Performance enhancement of TEC cooling	No comparison with solar-assisted absorption systems or practical economic analysis	Compares thermoelectric and solar-assisted cooling technologies under a unified assessment framework.
Present Study	Integrated technical-economic assessment of solar-assisted and thermoelectric air-conditioning systems	Mathematical modeling, experimental validation, TRNSYS simulation, EES analysis, and ETCC-based optimization	Addresses both technical and economic aspects simultaneously	Novel integrated framework combining solar-assisted absorption cooling and thermoelectric air-conditioning, experimental validation, optimization of collector area, storage tank, TEC configuration, operating current, and lifecycle cost. Provides practical design guidelines for sustainable residential cooling.

Research Gap

Despite significant progress in solar-assisted absorption cooling and thermoelectric air-conditioning technologies, several research gaps remain. Most previous studies have focused on either the thermal performance of solar-assisted absorption systems or the operational characteristics of thermoelectric cooling devices independently, with limited efforts toward integrating both technologies within a unified technical and economic assessment framework. Furthermore, existing research primarily emphasizes energy performance indicators such as cooling capacity and COP, while comparatively less attention has been given to comprehensive economic optimization that simultaneously considers investment cost, operating cost, and long-term system performance. In addition, many reported studies rely solely on numerical simulations without experimental validation of thermoelectric module characteristics, resulting in uncertainties in practical system performance. The optimization of key design parameters, including collector area, thermal storage capacity, number of thermoelectric

© STM Journals 2026. All Rights Reserved

modules, operating current, and heat exchanger characteristics under realistic residential operating conditions, has also received limited attention. Moreover, the practical feasibility of environmentally friendly air-conditioning systems that minimize electricity consumption and eliminate harmful refrigerants has not been comprehensively investigated. Therefore, there is a need for an integrated methodology that combines experimental validation, mathematical modeling, technical performance analysis, and economic optimization to support the design of sustainable and cost-effective air-conditioning systems.

Novelty of the Present Study

The present work addresses the aforementioned research gaps by developing an integrated framework for the technical and economic assessment of solar-assisted absorption and thermoelectric air-conditioning systems. The proposed methodology combines mathematical modeling, experimental characterization of commercially available thermoelectric modules, TRNSYS-based solar system simulation, EES-based absorption chiller modeling, and economic optimization using the ETCC criterion. The study further compares water-cooled and air-cooled absorption chillers, identifies the optimum collector area and thermal storage capacity, and determines the optimum operating conditions for thermoelectric cooling systems by considering both technical performance and life cycle cost. This comprehensive approach provides a practical guideline for designing energy-efficient, environmentally friendly, and economically viable residential air-conditioning systems. Comparative analysis of different studies mentioned in Table 1.

Development of a unified technical-economic assessment framework for both solar-assisted absorption and thermoelectric air-conditioning systems. Experimental characterization and validation of commercially available thermoelectric modules for accurate system modeling. Integration of TRNSYS and Engineering Equation Solver (EES) simulations for comprehensive system analysis. Introduction of the ETCC as an optimization criterion considering both investment and operating costs. Simultaneous optimization of solar collector area, thermal storage capacity, thermoelectric module configuration, operating current, and heat exchanger performance. Comparative evaluation of water-cooled and air-cooled LiBr–H_2O absorption chillers under identical residential operating conditions. Provision of practical design recommendations for energy-efficient, environmentally friendly, and economically viable residential air-conditioning systems.

MATHEMATICAL MODEL

LiBr-Water Absorption Machine

The operating principle of an absorption refrigeration system (Ta) resembles that of a vapor-compression refrigeration cycle, particularly in terms of its main components, namely, the evaporator and condenser. In the evaporator, the refrigerant (water) undergoes evaporation, thereby generating the desired cooling effect. The resulting refrigerant vapor (3) then enters the absorber, where it is absorbed by a concentrated lithium bromide (LiBr) solution returning from the generator (10) [18]. The diluted solution leaving the absorber (4) is subsequently pumped (5) through a regenerative solution heat exchanger, where it is preheated (6) before entering the generator. Within the generator, the solution is heated to a temperature above its boiling point, causing the refrigerant vapor to separate and be released (7). The concentrated solution (8) is then returned to the absorber. Meanwhile, the refrigerant vapor released from the generator (7) enters the condenser, where it undergoes condensation. The resulting liquid refrigerant (1) subsequently passes through an expansion valve, which lowers its pressure and causes partial evaporation, leading to a significant reduction in temperature. The refrigerant then enters the evaporator (2), where the evaporation process is completed, producing the desired cooling effect. Both the absorber and condenser may be cooled by air or water; when water cooling is employed, a cooling tower is typically required to sustain the heat rejection process [15]. In lithium bromide–water absorption chillers, salt crystallization can occur at high solution concentrations and low temperatures, particularly in the concentrated solution stream flowing toward the absorber after being cooled in the solution heat exchanger. As discussed later in this study, this issue can be prevented by identifying and maintaining suitable operating conditions within this section of the system, thereby ensuring that crystallization does not occur.

© STM Journals 2026. All Rights Reserved

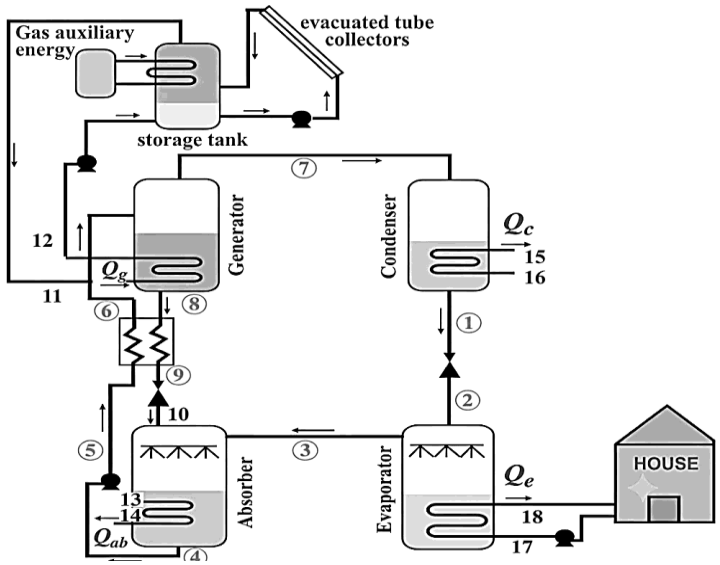


Figure 1. Solar-assisted air-conditioning installation using H_2O/LiBr absorption chiller [16].

The present analysis focuses on an air-conditioning system incorporating thermoelectric modules. It is assumed that heat reservoirs are located on both sides of the modules, with heat being transported to and from radiators by a circulating liquid that exchanges thermal energy with the surrounding environment. A schematic representation of the investigated air-conditioning system is shown in Figure 1. Based on this configuration, a mathematical model of the system was developed [11]. Owing to the thermoelectric Peltier effect, heat is extracted from the conditioned space at an indoor temperature T_{in} and transferred to the external environment at an outdoor temperature T_{out}. The processes of heat removal from the cooled space and heat rejection to the surroundings are governed by the heat transfer coefficients HTF_{in} and HTF_{out}, respectively. In practice, these two factors characterize the size and efficiency of the radiators. The heat absorbed on the upper side is then expressed as

$$\dot{Q}_{in}=HTF_{in}(T_{in}-T_u) \quad (1)$$

and the heat released to the outdoor environment is:

$$\dot{Q}_{out}=HTF_{out}(T_I-T_{out}) \quad (2)$$

Assuming that no heat losses occur within the liquid transport lines, the energy balance equations for the thermoelectric section of the system are represented by Equations (3) and (4). Figure 1 shows an enlarged view of a single pair of thermoelectric legs [13]. In practice, a thermoelectric module consists of numerous such couples electrically connected in series. Each couple is formed by two semiconductor elements that are electrically connected in series while remaining thermally connected in parallel. When an electric current passes through the thermoelectric couple, heat $\dot{Q}_{in}$ is absorbed at the upper surface, while heat $\dot{Q}_{out}$ is released at the lower surface owing to the Peltier effect.

Three primary phenomena govern heat transfer within thermoelectric modules: the Peltier effect**,** Joule heating, and thermal conduction. Among these, only the Peltier effect actively drives the heat-pumping process. As the Peltier heat absorbed at the upper thermoelectric junction is released at the lower junction, a temperature difference develops across the thermoelectric legs. This temperature gradient gives rise to the Seebeck effect**,** which generates an electrical voltage that opposes the Peltier-driven heat transport process. The temperature gradient across the thermoelectric legs also promotes heat conduction from the hot side to the cold side, thereby counteracting the desired heat-pumping action [19]. In addition, the electric current passing through the legs generates Joule heat as a result of the electrical resistance of the thermoelectric materials. This heat is produced throughout the entire volume of the legs and further reduces the overall performance of the module. Considering all of these phenomena—the Peltier effect, thermal conduction, and Joule heating—the energy balance equations

© STM Journals 2026. All Rights Reserved

for the upper and lower sections of the thermoelectric module can be expressed as follows:

$$\alpha I T_{ju} - \frac{I^2 R}{2} + k\left(T_{ju} - T_{jI}\right) = \frac{\left(T_u - T_{ju}\right)}{r_u} = \dot{Q}_{in} \tag{3}$$

$$\alpha I T_{jI} + \frac{I^2 R}{2} + k\left(T_{ju} - T_{jI}\right) = \frac{\left(T_{jI} - T_I\right)}{r_I} = \dot{Q}_{in} \tag{4}$$

where T_{ju}; T_{jI} are the upper and lower temperatures of the thermoelectric junctions, respectively; k is the leg thermal conductivity; α is the Seebeck coefficient; R is the electrical resistance; and I is the electric current.

Experimental Determination of the System Parameters

This section outlines the procedures used to determine the parameters of the TEC and the thermal contact conditions between the cells, which are essential for accurately modeling the performance of the proposed air-conditioning system [12]. Because the technical documentation provided by thermoelectric module manufacturers often lacks all the information required for detailed calculations, and because practical experience indicates that the parameters reported in datasheets do not always accurately reflect actual performance, experimental investigations were conducted. These tests were carried out to evaluate the module characteristics and to establish the thermal interaction conditions between the thermoelectric modules and the associated heat exchangers.

Test Stand

The subsequent analyses of the air-conditioning system were based on thermoelectric modules whose performance parameters were experimentally determined under actual operating conditions using commercially available devices. For this purpose, MCTE1-19913L-S thermoelectric modules, designed for refrigeration applications, were selected [20]. Because the internal construction details of the tested module were not available for this study, it was assumed that each module was composed of $(n = 105)$ thermoelectric couples, with each couple consisting of a thermoelectric leg pair.

Figure 2 presents a schematic representation of the proposed air-conditioning system. Electrical energy is supplied to the thermoelectric module, enabling it to transfer heat from the indoor environment HTF_{in} to the outdoor environment HTF_{out}. The rate of heat exchange between the system and its surroundings is regulated by heat transfer factors (HTFs). An enlarged view of a single thermoelectric couple is shown on the right side of the figure to illustrate the fundamental operating element of the thermoelectric module [21].

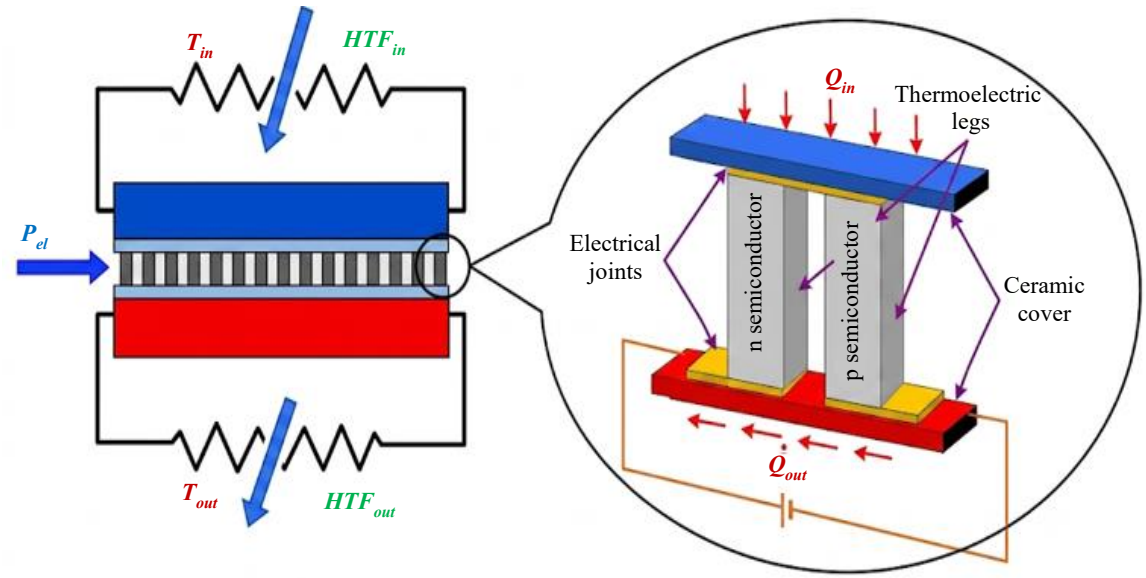


Figure 2. Schematic representation of the proposed air-conditioning system.

© STM Journals 2026. All Rights Reserved

Height h_ref=3 mm; all the parameters used in the calculations were determined based on this assumption. This assumption does not affect the accuracy of the obtained results. The parameters of the TEC were determined using a specially designed experimental test rig (Figure 2).

The setup consisted of two heat exchangers in the form of copper blocks, with the thermoelectric module positioned between them and secured using a controlled clamping force. Electric heating elements were embedded in the upper copper block, which represented the heat absorption side of the module. The lower heat exchanger, corresponding to the heat rejection side, contained internal cooling channels through which water circulated at a carefully regulated flow rate to remove the released heat. The experimental setup was extensively instrumented to measure and record both thermal and electrical parameters [22]. Among its capabilities, the test stand can operate under a constant temperature difference mode, in which electric heaters installed in the upper block are regulated by a proportional-integral-derivative (PID)controller to maintain a predefined temperature difference between the two blocks. The thermal contact conditions between the heat exchangers and the thermoelectric module influence thermal resistance at their interfaces and, consequently, have a significant impact on the module's performance. To minimize contact resistance and improve heat transfer, a layer of copper-based thermal grease was applied to the module surfaces during assembly.

Thermal Contact Resistance

The initial phase of the experimental investigation focused on determining the thermal resistance at the interfaces between the heat exchangers and the thermoelectric junctions of the TEC using the dedicated test rig described previously. During the tests, the lower heat exchanger was cooled by a continuous flow of tap water, maintaining its temperature within the range of 21–23°C. The electric current I=5A supplied to the TEC was directed such that the upper heat exchanger operated in cooling mode, while the lower heat exchanger functioned as the heat rejection side [23]. Throughout the experiments, several parameters were monitored, including the temperatures of the copper blocks, the thermal power supplied by the heaters required to maintain the prescribed temperature difference (ΔT) between the blocks, the steady-state voltage V_s, and the voltage measured immediately after disconnecting the electrical circuit of the thermoelectric module V_r.

The testing procedure takes advantage of the significant difference between the thermal and electrical response times of the thermoelectric module. Immediately after a change in the electrical condition from a short-circuit state to an open-circuit state, the temperature distribution within the module remains essentially unchanged for a few milliseconds because of its much greater thermal inertia. Consequently, the temperature field can be assumed to correspond to the preceding electrical operating condition [24]. Under steady-state conditions, the voltage V_r is directly proportional to the temperature difference across the thermoelectric junctions. The measured data and the parameters derived from these measurements are summarized in Table 1. All reported measurements were obtained under steady-state operating conditions, with the exception of V_r, which represents the voltage measured at the TEC terminals immediately after the electrical circuit is interrupted (within milliseconds) while the module remains in thermal steady-state. This measurement technique is commonly referred to as a rapid measurement.

The three measurements listed in the first three rows of Table 1 were conducted for small temperature differences between the blocks, ranging from approximately 8 K to 8 K. The values presented in the final row were obtained through linear regression of the experimental data [17]. It was assumed that, within the investigated temperature range, the variation of the analyzed parameters could be adequately described by a linear relationship with respect to the temperature difference between the blocks. This assumption implies that the thermoelectric properties of the TEC can be considered independent of temperature over the examined range. The experimental results confirmed the validity of this approximation. Using the linear approximation, it is possible to determine the temperature difference between the heat exchanger blocks at which the rapid measurement voltage $V_r = 0$ becomes zero. This condition indicates that the temperatures of the thermoelectric junctions are equal. Under these

© STM Journals 2026. All Rights Reserved

circumstances, no heat is transferred through the thermoelectric module by thermal conduction; therefore, the temperature difference between the heat exchangers, (ΔT), results solely from the thermal contact layers. Consequently, the average contact thermal resistance can be evaluated from the total heat flow passing through the two surfaces of the module [18].

$$\dot{Q}_{tot} = \dot{Q}_u + \dot{Q}_I \tag{5}$$

Dividing by the temperature difference makes it possible to calculate thermal resistance,

$$r = \frac{\Delta T}{\dot{Q}_{tot}} \tag{6}$$

Totaling $r = 0.070 K/W$. The thermal resistance was assumed to be identical on both sides of the module. The thermal resistance was assumed to be identical on both sides of the module. The calculated result represents the thermal resistance of a single contact layer [25]. The value of $\dot{Q}_u$ is known because it corresponds to the electrical power supplied to the heaters. The quantity $\dot{Q}_l$ can be determined from the energy balance by considering the Joule heat generated within the TEC, along with P_{el} and $\dot{Q}_u$. Furthermore, P_{el} can be obtained by multiplying the current (I) by the voltage (V).

$$P_{el} = IV_s \tag{7}$$

$$\dot{Q}_I = \dot{Q}_u + P_{el} \tag{8}$$

Solar Cooling System and Module Parameters

A solar-assisted air-conditioning system designed for a single-family residential building consists of three primary subsystems integrated with an absorption chiller.

- *Load subsystem:* This subsystem serves as the distribution network for the chilled medium, including the supply and return lines. It is connected to the delivery terminals installed in the conditioned spaces of the building (17 and 18) [26].
- *Cold production subsystem:* In this subsystem, the heat rejected by the absorber and condenser is transferred to the surroundings either directly through air-cooling or indirectly through a cooling tower in a water cooling arrangement. The cooling process first takes place in the absorber (13 and 14), followed by the condenser (15 and 16).

The heat production subsystem supplies the high-temperature thermal energy required by the thermally driven air-conditioning system through a heat exchanger (11 and 12). In addition to the solar collector array, the system includes several essential components, such as a thermal storage tank, circulation pumps, and thermostat controllers.

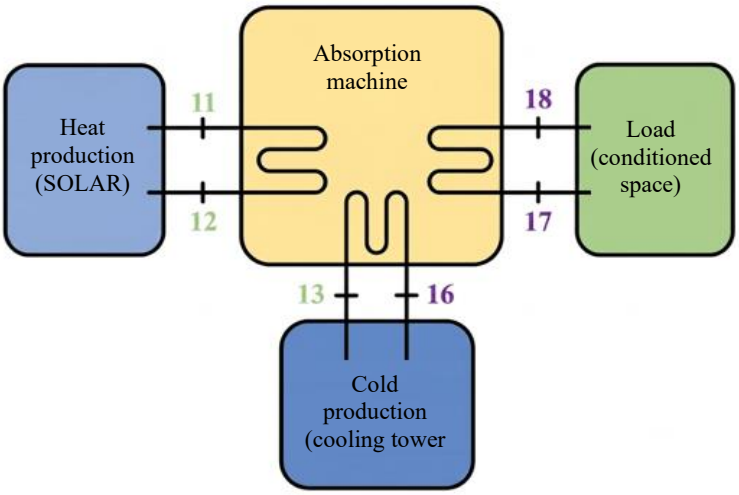


Figure 3. Schematic of the unit's connections of the solar-assisted air-conditioning system [27].

© STM Journals 2026. All Rights Reserved

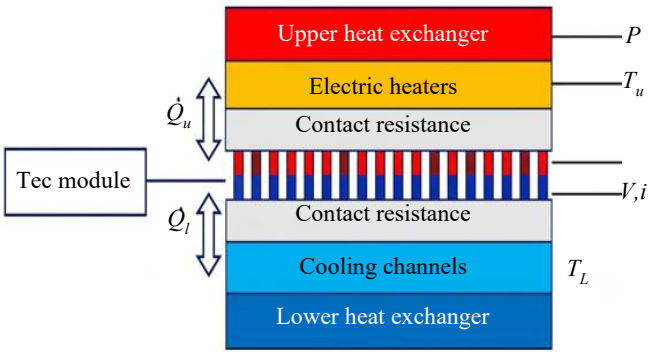


Figure 4. Schematic representation of the measurement system with an electrically heated upper heat exchanger at temperature $T_u$and a water-cooled lower heat exchanger at temperature T_l.

To satisfy the system's heat demand under conditions of insufficient solar radiation, limited collector area, or other operational constraints, an auxiliary heat source is integrated into the system. In the present study, a gas heater was considered as a supplementary source of thermal energy [28]. Using the average values of the voltage difference V_s-V_r and current, the internal electrical resistance of the TEC circuit (R-1.59Ω) can be readily determined.

Figure 4. The schematic of the measurement system consists of an upper heat exchanger maintained at temperature (T_u) and equipped with electric heaters, and a lower heat exchanger at temperature (T_l) containing cooling channels. A thermoelectric module is positioned between the two heat exchangers and is powered by an electrical supply. Thermal contact resistance is present at the interfaces between the thermoelectric module and the heat exchangers (V, I) [29].

Subsequent experiments were conducted with the temperature of the upper block maintained at 35°C to determine the Seebeck coefficient and thermal conductivity of the thermoelectric module. Under these conditions, attention was focused solely on the steady-state voltage produced by the module when the current in the TEC circuit was zero. The zero-current condition ensures the absence of Peltier heat generation [30]. Measurements were performed at two different cooling water mass flow rates, while the ambient temperature remained constant throughout all the tests: (T_u=24°C). The measurements initially enabled the determination of the heat loss coefficient to the surrounding environment. Throughout the experiment, the temperature of the upper block was maintained at a constant value by the electric heaters, whereas the temperature of the lower block varied with changes in the cooling water flow rate. Under steady-state conditions, no heat is converted into electrical energy; therefore, ($\dot{Q}_u$=$\dot{Q}_l$) the heat entering the system is equal to the heat leaving it [31]. Owing to the linear relationship between heat flow and temperature difference, linear approximation can be employed to estimate the heater power corresponding to the condition where the temperature of the lower heat exchanger becomes equal to that of the upper heat exchanger (T_u-T_l).

This procedure yields the value of $\dot{Q}_{loss}$~5W). By dividing (HTF_{loss}=0.45W/K) by the temperature difference between the upper block and the surrounding environment (T_u-T_a), the heat loss coefficient to the environment, ($\dot{Q}_{TEC}$=$\dot{Q}_u$-$\dot{Q}_{loss}$), can be determined for the measurement setup. Subsequently, the heat conducted through the thermoelectric module can be calculated as the difference between the heat supplied by the electric heaters and the heat loss to the surroundings [32]. The obtained heat loss value was then used to correct the calculated value of $\dot{Q}_{tot}$ as well as the previously evaluated contact thermal resistance. The correction was performed by adjusting the heat values, $\dot{Q}_u$, using a correction factor calculated from the current temperature of the upper block and the previously determined HTF_{loss} value. The experiments were then repeated with a different, high-quality thermal grease applied at the interface between the thermoelectric module and the heat exchangers. Consequently, the temperature difference corresponding to V_r=0 under the same operating condition was reduced to approximately 7 K,

© STM Journals 2026. All Rights Reserved

compared with the earlier value of 21 K. Consequently, the final value of the determined contact thermal resistance decreased significantly.

This result indicates that the high-quality thermal grease possesses an approximately threefold greater heat transfer capability compared with conventional copper grease; therefore, it was selected for subsequent calculations. The knowledge of the contact thermal resistance together with the heat flow through the thermoelectric cell makes it possible to determine the temperature difference deviation, defined as the difference between the measured temperature difference across the heat exchange blocks and the actual, unknown temperature difference at the thermoelectric junction [33]. This information forms the basis for evaluating the true temperature difference across the thermoelectric junction. The values obtained above enable the determination of the Seebeck coefficient by evaluating the ratio of the generated voltage to the temperature difference across the thermoelectric junction. Similarly, the thermal conductivity of the thermoelectric legs can be calculated as the ratio of the heat conducted through the cell to the temperature difference at the junction. For thermal analyses of an air-conditioning system, the influence of thermal radiation can be neglected because of the relatively low operating temperature range. Under these conditions, it is also reasonable to consider the thermoelectric module parameters to be independent of temperature, an assumption that has been experimentally verified.

The proposed methodology assists in:

- Reducing electricity consumption during peak cooling periods;
- Minimizing dependence on fossil fuel-based energy sources;
- Optimizing collector area and thermal storage capacity;
- Improving economic feasibility of solar-assisted cooling systems;
- Optimizing thermoelectric air-conditioning performance considering both capital and operating costs; and
- Providing an environmentally friendly alternative to conventional refrigeration systems.

VALIDATION

Solar Air-Conditioning System Analysis

The investigation of a solar cooling system is typically carried out through a structured, multistage approach that integrates thermal analysis, component-level modeling, system-level simulation, and economic evaluation. This step-by-step methodology ensures that both the technical performance and economic feasibility of the system are properly assessed before final design decisions are made [34]. The first step involves house cooling load assessment**,** which is performed using a built-in component of solar simulation software. In this stage, the cooling demand of the building is calculated based on several factors, such as building geometry, construction materials, insulation level, occupancy patterns, internal heat gains, and local climatic conditions. The objective is to determine the amount of cooling energy required to maintain indoor thermal comfort throughout different periods of the year. This load profile is essential because it serves as the foundation for designing the solar cooling system. An accurate estimation ensures that the system is neither undersized (leading to insufficient cooling) nor oversized (leading to unnecessary cost and inefficiency).

The second step is absorption machine modeling and simulation**,** which is carried out using an equation solver software. In this phase, the performance of the absorption chiller, a key component of the solar cooling system, is analyzed in detail. The absorption machine typically operates using a thermal energy source, such as hot water generated from solar collectors, instead of electricity [35]. Mathematical models representing heat and mass transfer processes within the absorption cycle are developed and solved. These models help determine important performance indicators such as the COP, cooling capacity, generator temperature requirements, and heat rejection loads. This step is critical for understanding how efficiently the absorption system converts thermal energy into cooling output under different operating conditions. The third step involves whole-system simulation using solar software**,** where all components of the solar cooling system are integrated into a single model. This includes solar collectors, thermal storage tanks, pumps, heat exchangers, and the absorption chiller. The system is

© STM Journals 2026. All Rights Reserved

simulated under real weather data to evaluate its dynamic performance over time [36]. This step helps in analyzing energy flows between components, solar fraction (the portion of cooling provided by solar energy), storage behavior, and system reliability. It also allows the identification of operational issues such as mismatch between solar energy availability and cooling demand.

The final step is a technical-economic analysis, which aims to optimize system design. This involves evaluating the cost-effectiveness of different configurations, particularly focusing on selecting the optimal solar collector area and system components. Key economic indicators, such as initial investment cost, operating cost, maintenance cost, and payback period, are considered. By comparing these against energy savings and system performance, designers can identify the most efficient and financially viable solution [37]. The goal is to achieve the best balance between energy performance and lifecycle cost. Overall, this four-step methodology ensures a comprehensive evaluation of solar cooling systems, combining engineering accuracy with economic practicality to support sustainable and cost-effective design decisions.

Cooling Loads Estimation

The building considered in this study has a total floor area of 170 m². It was simulated under Tunisian climatic conditions (Figure 3) and is represented as a multi-zone structure (Figure 4), consisting of three bedrooms, a living room, two bathrooms, and a kitchen. Each zone of the building was defined using TRNBUILD, which is a graphical user interface used to input data for multi-zone buildings modeled as 'TYPE56'. This interface allows detailed specification of the building structure, including all parameters required for thermal simulation. These parameters include the optical properties of windows, wall and layer compositions, construction types, as well as heating and cooling schedules, among other inputs necessary to accurately model the building's thermal performance [38]. Convective and radiative heat gains and losses were computed within TRNBUILD after defining the zone construction details. Several predefined input parameters and variables must also be specified, including occupancy, internal heat gains, comfort conditions, infiltration, ventilation rates, and weather data, among others. The cooling demand was determined by maintaining a set indoor temperature of 26°C throughout the summer period. This demand was evaluated by summing the instantaneous cooling loads of all conditioned spaces, including the three bedrooms, the living room, and the hall. The variation of the total cooling load over the summer period is presented in Figure 5. The results indicate that the building experiences a peak cooling load of 11.5 kW under hot summer conditions. To optimize energy use while maintaining nearly the same level of thermal comfort, it was assumed that the cooling system should satisfy 95% of the total cooling demand over the simulation period. Based on this assumption, the nominal capacity of the machine was determined to be 7 kW.

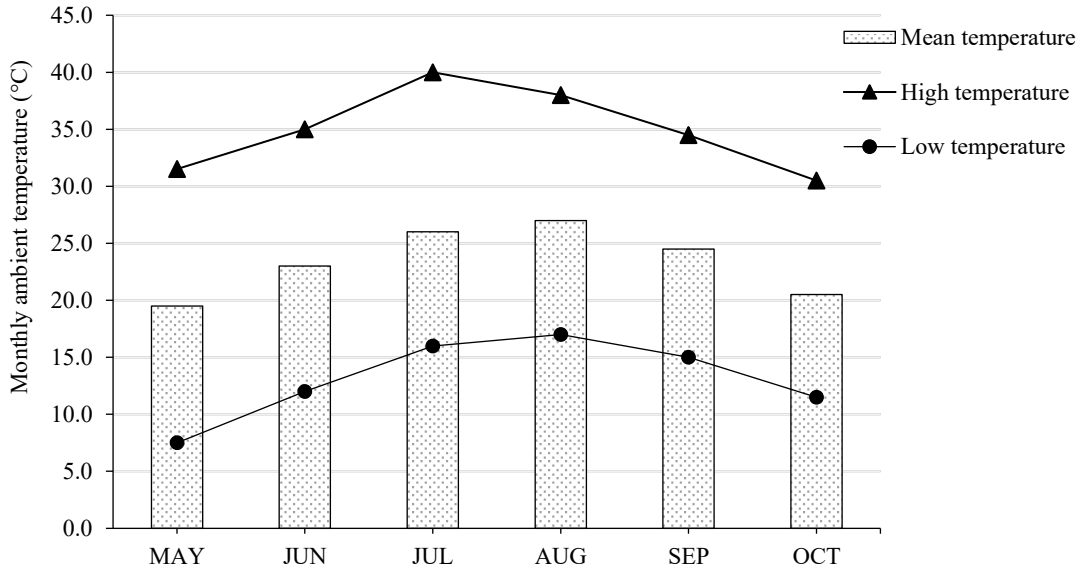


Figure 5. Monthly average temperature for City [39].

© STM Journals 2026. All Rights Reserved

Chiller Model and Simulation

To evaluate the performance of the chiller and understand how different component specifications influence its operation, a series of numerical simulations were conducted using an equation solver software. This step is essential in the design and analysis of thermal systems, particularly for absorption chillers, because their performance strongly depends on the interaction between multiple thermodynamic and heat transfer processes. Using an equation-based simulation approach, the system behavior can be studied under various operating conditions in a controlled and systematic manner [40]. The equation solver software allows the development of detailed mathematical models representing each component of the chiller, including the generator, absorber, condenser, evaporator, and solution heat exchanger. These components are interconnected through mass and energy balance equations, thermodynamic property relations, and heat transfer correlations. Once the governing equations are defined, the solver computes unknown variables such as temperatures, pressures, mass flow rates, and heat transfer rates simultaneously. This enables a comprehensive representation of the chiller's internal working mechanism.

One of the main objectives of these simulations was to evaluate the performance of the chiller**,** typically expressed in terms of the COP. The COP is a key indicator that relates the cooling output to the thermal energy input supplied to the generator [41]. By varying the input conditions, such as generator temperature, cooling water temperature, and chilled water outlet temperature, the sensitivity of the COP and cooling capacity can be analyzed. This helps identify the optimal operating range of the chiller, where efficiency is maximized. In addition to the performance evaluation, the simulations were also used to study the effect of component specifications on system behavior. Parameters such as heat exchanger effectiveness, solution concentration, flow rates, and heat transfer coefficients were systematically varied. These variations allow researchers to understand how improvements or limitations in individual components influence the overall system performance. For example, increasing the effectiveness of the solution heat exchanger may reduce thermal losses and improve COP, while poor heat transfer performance in the absorber or condenser may significantly reduce the cooling output.

Another important aspect of these simulations is the ability to perform parametric analysis and optimization. By running multiple simulation cases with different design configurations, it is possible to identify the most efficient combination of parameters. This helps in selecting appropriate component sizes and operating conditions before physical implementation [42]. It also reduces experimental cost and time by limiting the need for extensive prototype testing. Furthermore, the simulation results provide valuable insights into the dynamic behavior and stability of the chiller system. Even though many equation solvers operate under steady-state assumptions, they still allow the examination of system responses under varying loads and boundary conditions. This is particularly important for solar-driven cooling systems, where the thermal input fluctuates throughout the day.

Machine Model

Mathematical models for the different system components, namely, the absorber, generator, condenser, evaporator, solution heat exchanger, solution expansion valve, pump, and throttle, have been provided [43]. The basic mass and energy conservation equations applicable to each component are formulated as follows:

Mass balance

$$\sum m_{in} = \sum m_{out} \tag{1}$$

$$\sum m_{in} x_{in} = \sum m_{out} x_{out} \tag{2}$$

Energy balance

$$Q_i = \sum m_{in} h_{in} - \sum m_{out} h_{out} \tag{3}$$

$$Q_i = (UA)_i (LMTD)_i \tag{4}$$

© STM Journals 2026. All Rights Reserved

Cycle Simulation

Water-Cooled Chiller

The nominal operating conditions and heat transfer characteristics of the various machine components are presented. A preliminary analysis was conducted to evaluate the influence of the generator inlet temperature and flow rate on machine performance (Figure 6) [44]. These parameters determine the thermal power requirements of the generator. The results indicate that the COP increases with increasing generator temperature, reaching a maximum value of 0.7.

Small variations in the hot water generator temperature led to a sudden reduction in cooling capacity. To avoid oversizing the machine, the selection of the hot driving temperature is mainly based on the chiller cooling capacity of 7 kW. Figure 7 indicates that a hot water temperature of 98°C, which provides a cooling capacity of 7 kW, is suitable.

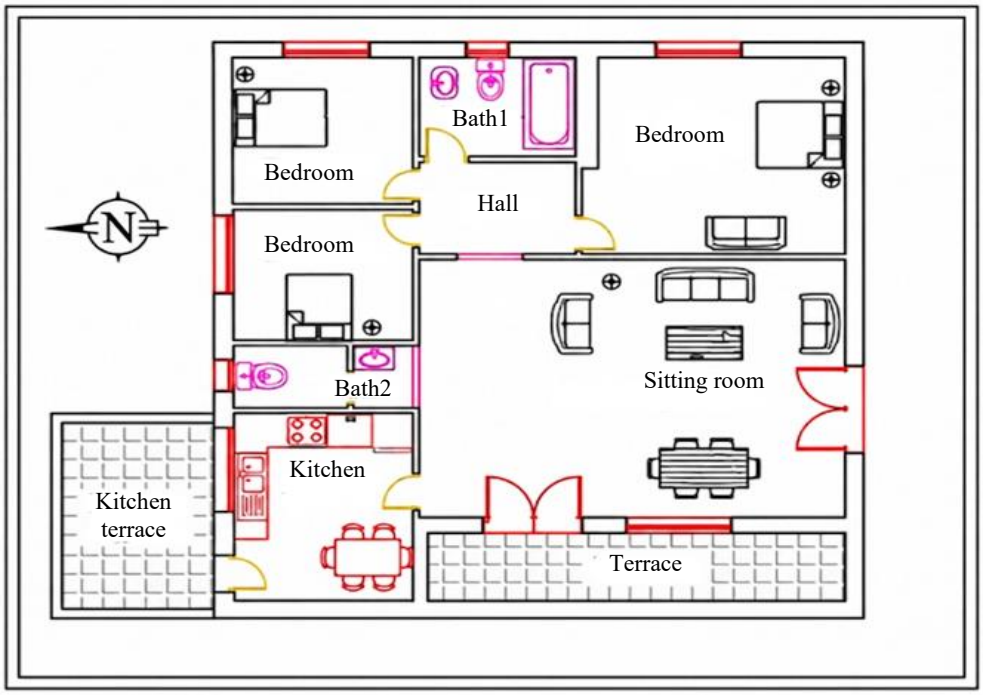


Figure 6. Plan view of the house [45].

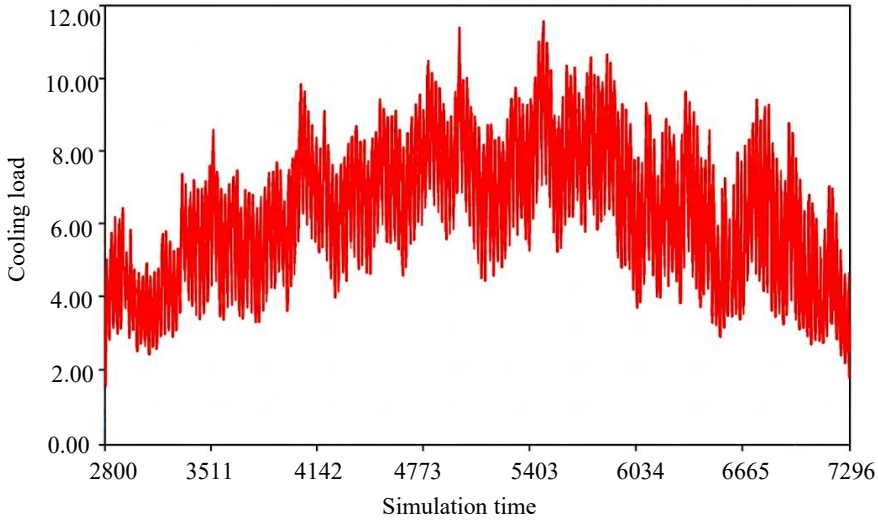


Figure 7. Building cooling loads during the summer simulation period [46].

© STM Journals 2026. All Rights Reserved

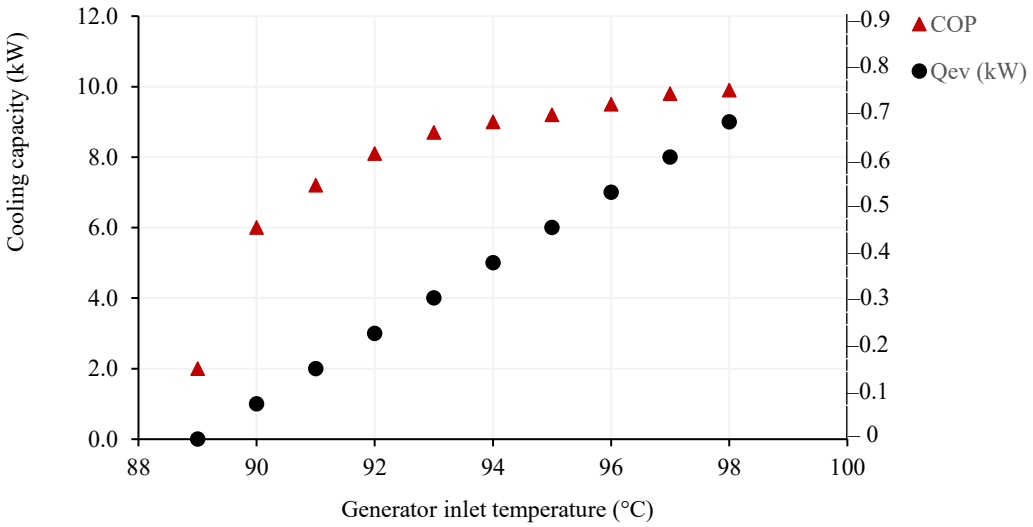


Figure 8. Effect of the generator inlet temperature on the performance of the absorption chiller [47].

Air-Cooled Chiller

The air-cooled machine was assumed to operate under the nominal conditions listed in Table 1. When the chiller is directly cooled by hot ambient air during the simulation period extending into summer, where temperatures may exceed 40°C (Figure 8), the risk of crystallization in the solution heat exchanger may increase. Therefore, the evaporation temperature was set to 10°C instead of 5°C, as used in the water-cooled machine. Air-cooled absorption machines also require a higher condensation temperature compared to water-cooled systems [48, 49]. Thus, the required hot water driving temperature in the generator exceeds 98°C.

Furthermore, if the pressure in the solar pipelines is restricted to 2.5 bar, the corresponding boiling temperature of water is 120°C. Therefore, the generator temperature range must be maintained between 98°C and 120°C. These relatively high temperatures in the generator and absorber increase the likelihood of salt precipitation. Crystallization must be prevented, as it can lead to sludge formation and may ultimately cause complete flow blockage if the mixture solidifies. Therefore, all these constraints must be considered when defining the operating conditions of the air-cooled chiller. Figure 9 presents a comparison of the temperature, pressure, and concentration characteristics of the thermodynamic cycle for two ambient air temperatures (35°C and 40°C) and two generator inlet temperatures: 105°C (a) and 115°C (b). These results show that an increase in the cooling medium temperature shifts the cycle closer to the crystallization limit curve. Conversely, a driving hot water temperature of 105°C and, more effectively, 115°C, moves the cycle trajectory away from the crystallization boundary for both ambient air conditions [50]. Accordingly, a generator inlet temperature of 115°C was selected for subsequent analysis.

Solar Cooling Simulations

TRNSYS System Description

Within the TRNSYS environment, the solar air-conditioning system simulation consists of interconnected subsystems. Each industrial component is identified by a "Type" number (for example, Type 56) and corresponds to a model block programmed in FORTRAN, containing defined inputs, outputs, and parameters, thereby functioning as a FORTRAN subroutine [51].

Simulation results

The analysis was carried out using typical meteorological data for a city classified under the Mediterranean climate. The solar subsystem included a 1.260 m³ hot water storage tank for the water cooling mode and a 0.980 m³ tank for the air-cooling mode, an evacuated tube collector field inclined

© STM Journals 2026. All Rights Reserved

at 36° to the horizontal, and a thermal backup source provided by a gas heater. The specific water flow rate was maintained at 80 L/h·m². The effect of collector surface area on solar gains and auxiliary heat demand was investigated (Figures 9 and 10) [52]. The pressurized water used to heat the generator was maintained at 98°C for the water cooling configuration and at 115°C for the air-cooling configuration. As anticipated, increasing the collector area resulted in higher heat collection and reduced auxiliary energy requirements. The auxiliary heat demand ranged from 6,695 to 13,335 kWh for the water-cooled system and from 8,406 to 13,023 kWh for the air-cooled system.

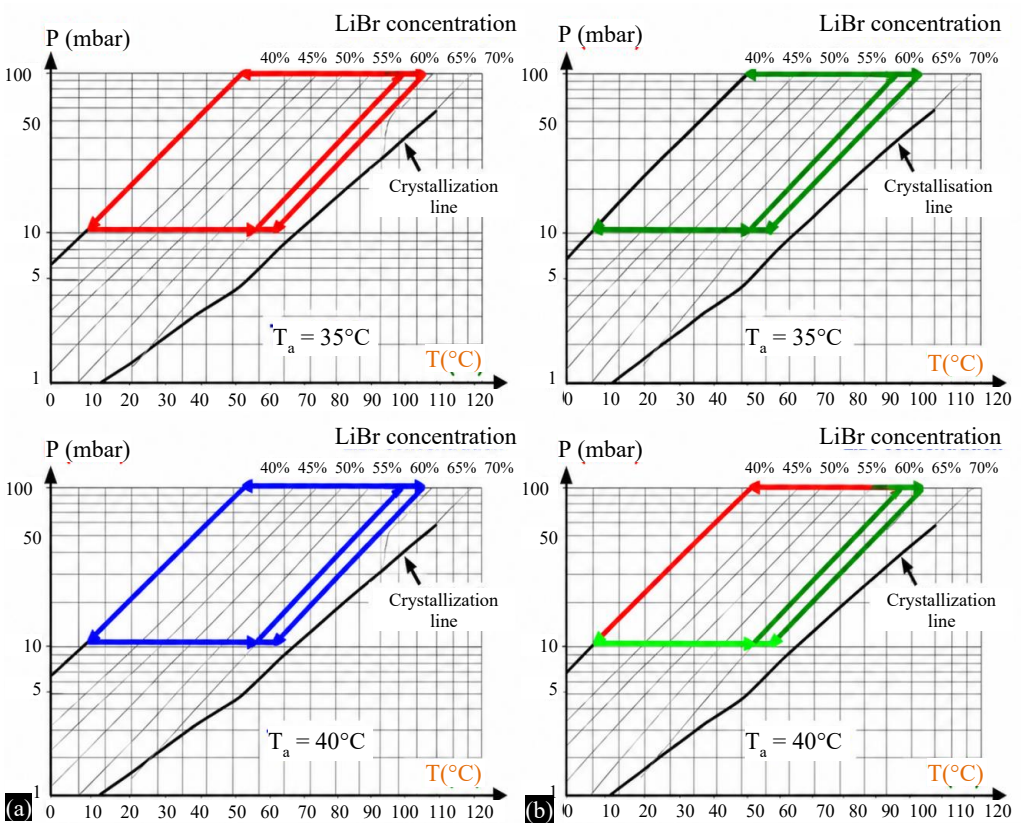


Figure 9. Cycle plots for two levels of ambient air (37°C and 42°C) [48].

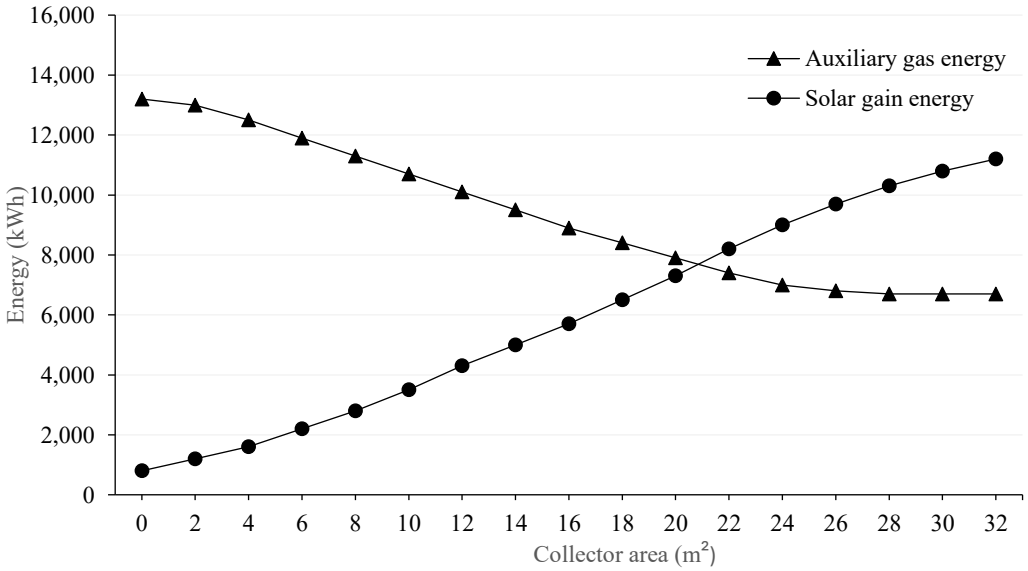


Figure 10. Solar and gas energy needs for water cooling vs. collector area [53].

© STM Journals 2026. All Rights Reserved

Figure 11 illustrates the variation of the solar fraction *f* with respect to the collector surface area. The solar fraction, defined as, is calculated based on the auxiliary heat supplied by the backup heater Q_{gas} required to meet the total energy demand of Q_g the heat production subsystem feeding the machine generator. It is observed that the solar fraction increases as the collector area increases [54–57].

$$f=1-\frac{Q_{gas}}{Q_g} \tag{5}$$

However, the auxiliary energy does not become zero even when the solar contribution approaches 90% of the system's energy demand. Therefore, in all cases, additional fossil fuel-based backup energy is required to maintain the pressurized water temperatures of 98°C for the water cooling mode and 115°C for the air-cooling mode. The technical analysis presented above is not sufficient to determine the optimal collector area for the solar air-conditioning system, as economic factors have not yet been considered [57].

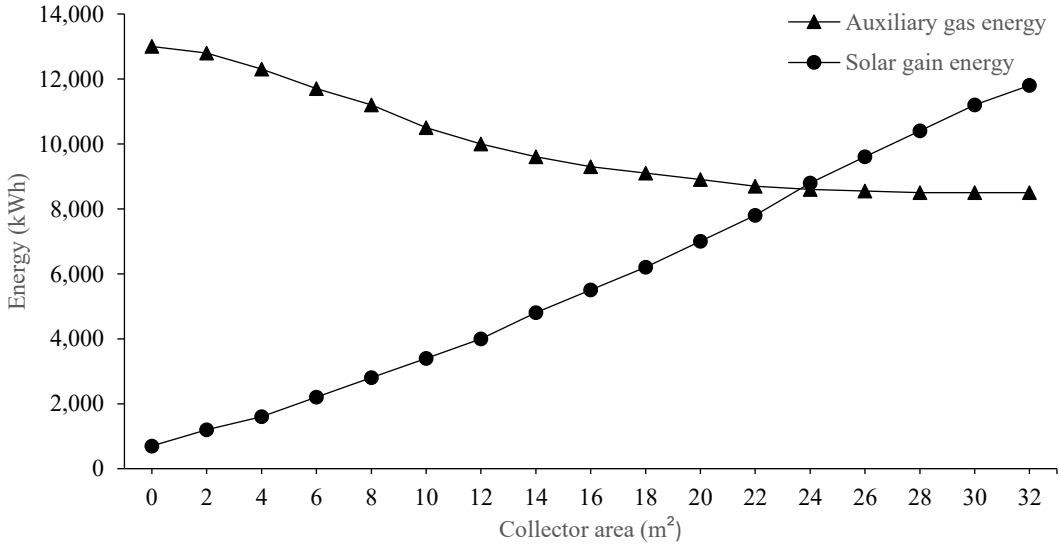


Figure 11. Solar and gas energy needs for air-cooling vs. collector area [55].

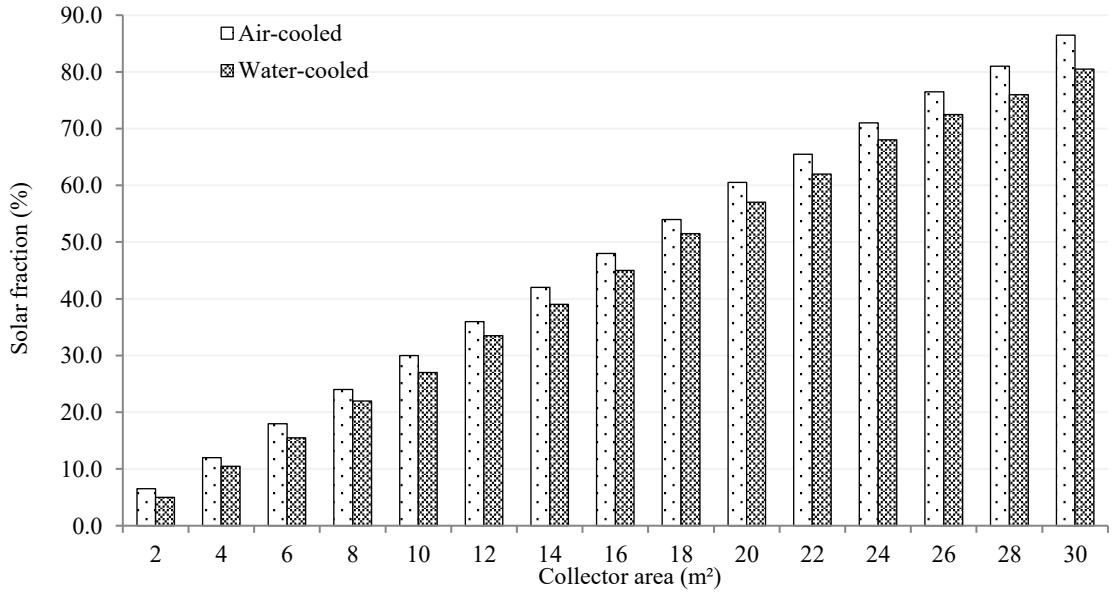


Figure 12. Solar fraction versus collector area [56].

© STM Journals 2026. All Rights Reserved

Technical and Economical Optimization

A cost-performance analysis was conducted to evaluate the economic feasibility of the project. The most comprehensive method for analyzing solar process economics is the life cycle cost approach. This technique enables comparison of future costs with present values by incorporating the time value of money, thereby allowing a detailed assessment of the full range of expenditures involved. The annual costs were determined by listing all expected expenses and discounting them to their present value. To simplify the system configuration, the total cost excludes the components connected to the delivery terminals located in the conditioned space, as the load subsystem is common to all comparable projects [58]. The discounted total annual cost of the entire plant was obtained as the sum of four components: chiller cost, solar system cost, auxiliary gas energy cost, and the cost associated with solar fraction cooling water production. Initially, the discounted annual total cost discounted annual total cost (CATD) was calculated for each component by adding all discounted investment costs of the system elements, amortized over an expected lifetime of 20 years, along with the discounted annual expenses discounted annual expenses (CAD). These annual expenses include maintenance and inspection costs maintenance and inspection costs (CM), estimated at 2% of the investment cost, and operating energy costs operating energy costs (CE) (gas consumption costs).

The analytical model and the corresponding software developed for performing the analyses were experimentally validated using a purpose-built specialized measuring stand. The details of the stand structure and its testing capabilities are provided. The stand consists of two copper blocks, which function as the heat sink and the cooled space, respectively. The first block contains cooling channels through which water flows, while the second block is equipped with electric heaters (see Figure 12). The thermoelectric module under test was positioned between these two blocks [59]. The validation experiments were conducted using another specimen of the MCTE1-19913L-S module type employed in the analyses. The contact surfaces between the module and the blocks were coated with high-quality thermal paste. Initially, the parameters of the tested module specimen and the operating conditions of the thermoelectric system were established. The only parameter showing a noticeable difference between the TEC specimens was the Seebeck coefficient, which varied by up to 10%. The validation tests involved allowing the system to reach steady-state conditions at a specified mass flow rate of water used to cool the lower block. The upper block was heated using electric heaters regulated by a PID controller to maintain a constant temperature equal to the ambient environment. This condition ensures that no heat is lost to the surroundings. Under steady-state conditions, the electrical power supplied to the heaters equals the cooling power produced by the module for a specified supply current and a defined temperature difference across the modules. Consequently, there is no requirement to measure the cooling water mass flow rate; only the temperature of the lower block needs to be recorded. These measurements were performed for various values of the cooling water mass flow rate and different module supply currents. It should also be noted that measuring current and temperature is straightforward, and the obtained results are associated with only a small error [60]. In this study, temperature was recorded using PT100 resistance thermometers, which offer high absolute measurement accuracy (below 0.5%). Electrical power was measured using an EA-PSI 9200–25 T laboratory power supply with an accuracy of 0.4%. The calculated cooling power shows a maximum deviation of approximately 6%, while the average difference remains below 4%. Despite the one-dimensional assumption of the model, the experimental results indicate that the influence of spatially distributed phenomena is relatively minor.

PERFORMANCE SIMULATIONS OF THE SYSTEM

TEC Module Characteristic Curves

Initially, the characteristics of the analyzed single stand-alone thermoelectric module were established. For this purpose, it was assumed that the radiator temperatures were steady and predefined for each point used in determining the characteristics. The upper radiator temperature was kept constant at 25°C in all cases. It was also assumed that at the interface between the thermoelectric junction and the heat-transporting fluid, the thermal resistance per unit area was estimated, consisting of the contact

© STM Journals 2026. All Rights Reserved

thermal resistance at the TEC interface and the thermal resistance between the heat exchanger and the liquid flow [61]. This value was also used in subsequent simulations. The cooling power and COP were computed over a wide range of supply currents to the thermoelectric module for different temperatures of the lower radiator. As the temperature difference increases, the range of currents for which positive cooling power can be achieved becomes narrower. It can be observed that the red line connecting the maximum cooling power points for a given temperature difference corresponds to an almost constant current, slightly above 11 A. By analyzing the maximum COP curve (the red line passing through the peak values), where the COP is defined as the ratio of cooling power to electrical input power, it is observed that the maxima shift toward lower current values. COP values greater than 3 can only be achieved when the temperature difference is below 8 K, and the current is less than 3 A [62].

Characteristics of the Air-Conditioning System

At this stage, the characteristics of the radiators were incorporated into the analysis. It was initially assumed that the radiator on the heat rejection side (outdoor) was twice the size of the radiator on the heat absorption side (indoor). In addition, both radiators were equipped with fans to enhance heat transfer [63]. Therefore, the heat transfer conditions were estimated at the levels of $HTF_{in} = 100W/K$ and $HTF_{out} = 200W/K$, where $100W/K$ is equivalent to a single computer cooler. The analysis focused on the steady-state performance of an air-conditioning system employing the previously tested TEC under the specified heat transfer conditions $HTF_{in} = 100W/K$ and $HTF_{out} = 200W/K$. Simulations were performed to examine the cooling power and COP achieved at different supply currents of the thermoelectric module for two selected temperatures of the lower (outdoor) heat reservoir: 25°C (0 K temperature difference) and 30°C (5 K temperature difference). During these simulations, the temperature of the upper (indoor) heat reservoir was maintained constant at 25°C. The results presented above indicate that a single thermoelectric module provides relatively low cooling power [64]. Therefore, an alternative configuration was investigated, involving the parallel thermal connection of 10 modules (n =1000).

The results are presented on a per module basis for the 10-module system. The cooling power curves indicate that, in every case, a maximum cooling power is achieved at a particular current value. For the 10-module configuration, the plotted curves exhibit a lower peak cooling power, and this peak occurs at a lower current. This behavior is attributed to the quantity of heat exchanged with the surroundings, as the same radiators were used in both configurations involving one module and ten modules. In the latter configuration, the radiators are unable to provide adequate heat transfer to fully exploit the cooling capacity of such a large number of thermoelectric modules. As a result, the temperature difference between the two sides of the modules increases excessively. Reduced heat dissipation requires a lower TEC supply current because of the balance between the Peltier effect and Joule heating. Any further increase in the number of modules would intensify this effect and lead to a continuous decrease in the COP [65]. It should be noted that an increase in the total module surface area results in a reduction in the overall contact thermal resistance, thereby decreasing the temperature difference between the thermoelectric junction and the corresponding heat reservoir for a constant heat flow. Furthermore, increasing the number of TECs enhances heat conduction through the modules, which may further reduce the temperature difference between the thermoelectric junctions. The factors that reduce the cooling power of the 10-module thermoelectric system (when normalized per module) also contribute to a lower overall system efficiency. Under zero-temperature-gradient conditions, the COP increases as the current flowing through the circuit decreases. However, when a temperature gradient exists, the behavior changes. At low current levels, the COP becomes negative because the heat flow occurs in the opposite direction. Only when the current is sufficiently increased does the Peltier effect become strong enough to reverse the heat flow direction and produce cooling in the upper heat reservoir.

Impact of the Number of Thermoelectric Modules on the System

In the next stage, the effect of the number of TEC modules used in the system on the cooling

© STM Journals 2026. All Rights Reserved

performance was examined. To ensure sufficient coverage of the design space, the number of thermoelectric legs was selected as a variable parameter and varied in increments of 20. The electrical current supplied to TECs was considered as the second variable. By exploring the design space over practical ranges of current and thermoelectric system size (number of legs), contour plots were generated to illustrate the cooling power and COP. It was assumed that only configurations capable of delivering cooling power greater than 250 W are of practical interest [66]. Under the adopted assumptions, the maximum cooling power achieved by the analyzed system was 913 W. This corresponds to a configuration with 35–36 reference modules (equivalent to the specified number of legs) operating at a supply current of 6.3 A. The contour levels of cooling power exhibited oval-shaped patterns, with a greater elongation along the axis representing the number of legs. This indicates that a similar maximum cooling capacity can be achieved across a relatively broad range of thermoelectric module quantities.

It can also be inferred from the chart that smaller thermoelectric systems provide a wider range of current variation while maintaining similar cooling power levels. In contrast, larger systems require more precise current adjustment to achieve the desired cooling capacity. The maximum COP reached a value of 2.28 for the configuration with the specified number of legs, operating at a current of 1.8 A. This value lies at the boundary of the considered domain and results directly from the imposed constraint on the solution space, namely a minimum cooling power of 250 W. At the point of maximum cooling power, the COP is 0.42 [67]. Although higher COP values can be observed in the graph, they are associated with very low cooling power outputs and therefore fall outside the region of practical interest. The results once again highlight the trade-off between cooling power and COP within the operating range considered. Since the maximum COP is influenced by the minimum cooling power assumed for the system, the following graph illustrates the relationship between these two parameters. Additionally, the required number of TEC modules and their corresponding supply current are provided for each case presented. Figure 12 shows that increasing the minimum cooling power requirement of the system leads to a reduction in cooling efficiency. It also necessitates a greater number of thermoelectric modules operating together (as indicated by the marker size and number) and requires a higher supply current to power them.

ECONOMIC OPTIMIZATION OF THE AIR-CONDITIONING SYSTEM

The next phase of the air-conditioning system study involved an economic assessment of the system. Based on available market data, the actual cost of a thermoelectric leg was assumed to be cost of a thermoelectric leg (NTEC), corresponding to 1% of the price of a reference 100-leg module. Similarly, the unit cost of the radiators, estimated to be using a 360 mm 15 FPI cooler as reference, was taken as unit cost of a radiator (NR). This estimation was based on commercially available computer cooling radiators. The cost of electricity required to power the thermoelectric module was also considered [68]. The cooling power (left) and COP (right) are presented as functions of the number of thermoelectric legs and the supply current. The values indicated at the markers represent the corresponding number of modules. For a specified minimum cooling power requirement, the appropriate size of the thermoelectric system, the corresponding COP, and the optimum supply current can be determined. It was further assumed that the device operates for 8 h per day over 60 days annually, resulting in a total operating time of 480 h per year. The calculations were conducted for a service life of 5 years, corresponding to 2400 operating hours. Based on the above assumptions. It should be noted that the value of (P_{el}) depends on the number of thermoelectric modules, the electrical current supplied to the circuit, and indirectly on the temperatures at both sides of the modules.

It is assumed that heat transfer on both sides of the system is achieved using radiators with the same unit cost, NR. The cost of the thermoelectric modules is considered to comprise 80% manufacturing expenses and 20% thermoelectric material costs, with the latter incorporated in the final term of Equation (10) through the ratio of leg heights. To achieve minimum cost, the system was subjected to

© STM Journals 2026. All Rights Reserved

an optimization process [69]. The design variables selected for optimization were the radiator dimensions, represented by HTF, and the current supplied to the modules. ETCC represents the ETCC and denotes the cooling power obtained per dollar of the total system cost. The total cost includes both the electricity consumption cost and the purchase cost of the device. The objective of the optimization was to maximize the ETCC value. The objective function consists of two components: the first component, ETCC, is the parameter directly maximized, while the second component is introduced to impose a constraint related to the cooling power of the system. During the optimization process, when only the first term of the objective function was considered, several similar optimum solutions were obtained for different combinations of the design variables.

Therefore, an additional term was incorporated into the objective function that slightly favored solutions with higher cooling power values, with its influence on (G) limited to approximately 1%. Owing to the stepwise variation of the parameter (g), a greater pressure was applied during the initial stage of the optimization process, thereby improving convergence [70]. As a result, the solutions obtained became stable and reproducible. Furthermore, when two configurations yielded the same ETCC value, the configuration with the higher cooling power was regarded as superior. Such a system, for a given number of modules or cooling capacity, possesses a higher power-to-size ratio, which also contributes to lower secondary costs that are not explicitly considered in the optimization, including expenses associated with casing fabrication, packaging, transportation, and ease of operation. Using the conditions defined in this manner, simulations were carried out for an air-conditioning system consisting of 10 basic TEC modules with the specified thermoelectric leg height. The supply current and both HTF values were selected as the design variables. Under these conditions, the final term of the objective function (F) in Equation (10) remained constant [71]. The resulting contour map illustrates the cooling power obtained per unit investment and total operating cost ($ 1) as a function of electricity cost and outdoor temperature.

A Device with the Design Cooling Power of 2 kW

The optimization results presented above do not consider the actual cooling power delivered by the system under specific operating conditions. Therefore, in the next stage, the required number of basic thermoelectric modules was determined to provide a dependable cooling capacity of 2 kW, which is a typical power rating for portable air-conditioning units used in small rooms. The device was assumed to operate at the maximum ETCC value [72]. At this stage, the number of thermoelectric legs (n) was introduced as an additional variable in the objective function, while the subsequent calculations continued to be based on the reference leg height, which remained constant. Although increasing the current supplied to the thermoelectric modules can enhance performance, operating the system under such conditions moves it beyond the optimum ETCC point, making the operation less economically efficient. The results indicate that, under the reference conditions, achieving the required cooling power necessitates the use of 4140 thermoelectric legs, corresponding to approximately 41 basic reference modules. For this configuration, the required supply current was approximately 5 A.

Within the analyzed range of parameter variations, the number of required modules ranges from 30 to 60, leading to different proportions of investment and operating costs in the total expenditure. As the cost of electricity increases, the required number of modules also increases, resulting in higher initial investment costs. The required number of modules also increases with a rise in the temperature difference, although the rate of increase is lower than that observed for operating costs [73]. Employing a larger number of modules makes it possible to achieve the desired cooling capacity through the Peltier effect while operating at lower current levels. However, Joule heating, which is an undesirable effect, increases in proportion to the square of the current, whereas the Peltier effect varies directly with the current. Consequently, the use of a greater number of modules may appear economically advantageous. However, it should also be recognized that increasing the number of modules results in greater heat conduction through the thermoelectric legs, which adversely affects the overall performance and efficiency of the system. In addition, the cost of each thermoelectric module also influences the overall system economics. Further contour maps were generated for the analyzed 2 kW cooling system. These

© STM Journals 2026. All Rights Reserved

maps illustrate the HTF values of both the indoor and outdoor radiators under different operating temperatures and varying electricity cost levels. HTF coefficients directly affect the size and/or performance quality of the radiators on both sides of the system and, consequently, have a significant impact on their overall cost.

Up to this point, the optimal design and operating parameters of the system have been determined for each operating condition defined by the cooling power, indoor–outdoor temperature difference, and cost of electricity [74]. However, an important question remains regarding how variations in operating conditions, such as changes in outdoor temperature or electricity price, would influence the ETCC. While adjusting the supply current of the system can be accomplished relatively easily, modifying the physical design of an existing system appears to be impractical and economically unjustifiable. To evaluate the extent of ETCC variation resulting from changes in the conditions, simulations were conducted for a system optimized under the reference operating parameters. In this case, the design characteristics and structural features of the system were kept fixed, while the supply current was optimized to maximize the ETCC. Figure 12 illustrates the percentage variation in ETCC (left) and cooling power (right) of the device as functions of changes in electricity cost and outdoor temperature. The system was optimized at the reference operating point to achieve the maximum ETCC [75]. As shown in the graph, an increase in outdoor temperature of less than 5 K results in an ETCC reduction of less than 1%, while the cooling power decreases by approximately 5%. Across the entire range considered, the variation in ETCC remains below 10%, whereas the cooling capacity can decrease by as much as 25%.

Impact of a Change in Leg Height

The height of the thermoelectric legs within the module influences both the operating characteristics of the TEC and, to some extent, the manufacturing cost. Variations in leg height primarily affect the amount of heat conducted through the module, the level of Joule heat generated, and the quantity of thermoelectric material required for fabrication [76]. Accordingly, simulations were conducted to evaluate the ETCC of the air-conditioning system while accounting for variations in thermoelectric leg height. As a result, the objective function (10) now includes an additional design variable, h. It is assumed that the thermoelectric material contributes 20% of the TEC module manufacturing cost, while the remaining 80% corresponds to other manufacturing expenses, as represented by the factors 0.2 and 0.8 in Equation (10). The reference leg height corresponds to the basic module model with a known purchase cost. As the cost of electricity increases, a larger number of modules become preferable because of the reduced proportion of investment cost in the total expenditure and the possibility of operating at a lower supply current. The above calculations correspond to a scenario in which variations in leg height result in a proportional change in the thermoelectric module cost, with the thermoelectric material accounting for 20% of the module cost relative to the reference module [77]. The indoor temperature was maintained at 25°C. Higher HTF values indicate the use of larger and more costly radiators. The percentage deviations of ETCC and cooling power from their optimal values at the reference operating point were evaluated for changes in outdoor temperature and electricity cost. At the reference point itself, no deviation is observed.

The HTF coefficients and number of modules were kept identical to those at the reference operating point, while the electric current was re-optimized for each case. ETCC decreases as the operating conditions move away from the reference point. For modules with a reference leg height of 3 mm, it can be observed that the system exhibits greater sensitivity to variations in both outdoor temperature and electricity cost. Within the considered range of temperature and cost variations, an increase of up to 35% in ETCC and a reduction of up to 55% in cooling power may be observed [78]. This indicates that a system optimized for specific predetermined operating conditions (the reference point) achieves superior ETCC under design-state operation. However, any departure from these conditions leads to a more rapid decline in the performance of this parameter.

© STM Journals 2026. All Rights Reserved

CONCLUSION

This study presents a comprehensive technical and economic assessment of solar-assisted absorption and thermoelectric air-conditioning technologies for residential applications through an integrated modeling, simulation, experimental validation, and optimization framework. Unlike previous investigations that mainly focused on either technical performance or economic evaluation separately, the proposed methodology simultaneously considered cooling performance, energy utilization, system cost, and long-term operational feasibility using the ETCC criterion. The simulation results demonstrated that the optimum water-cooled absorption chiller configuration requires an 18 m^2 evacuated tube solar collector and a 1.26 m^3 thermal storage tank, supplying approximately 55% of the cooling energy demand. The air-cooled configuration achieved optimum performance using a 16 m^2 collector field and a 0.98 m^3 storage tank, providing nearly 45% solar energy contribution. Although the solar-assisted system involves a higher initial investment than conventional vapor-compression systems, it substantially reduces electricity consumption, fossil fuel dependency, and the use of environmentally harmful refrigerants, making it an attractive solution for sustainable residential cooling. Experimental characterization of commercially available thermoelectric modules enabled accurate modeling of the proposed thermoelectric air-conditioning system. The developed mathematical model, validated experimentally, demonstrated that the cooling performance depends strongly on the number of thermoelectric modules, operating current, and heat exchanger characteristics. Economic optimization based on ETCC showed that operating the system at the maximum cooling capacity is not economically optimal. Instead, an optimized operating point provides the best compromise between cooling performance and lifecycle cost, while the system can tolerate approximately 32% overload under reference operating conditions without significantly affecting its economic performance. The principal novelty of this work is the development of an integrated technical-economic framework that combines experimental validation, mathematical modeling, TRNSYS-based solar simulation, EES-based absorption chiller analysis, and ETCC-based optimization for evaluating both solar-assisted and thermoelectric air-conditioning systems within a single study. This integrated methodology fills an important research gap by providing simultaneous technical and economic optimization rather than evaluating these aspects independently. From a practical perspective, the proposed approach offers valuable design guidelines for engineers, researchers, and policymakers involved in sustainable building technologies. The methodology can assist in selecting optimal collector areas, thermal storage capacities, thermoelectric module configurations, and operating conditions for residential cooling systems while improving energy efficiency and reducing greenhouse gas emissions. The proposed framework can also support the wider adoption of renewable-energy-based cooling technologies in regions experiencing high cooling demand and increasing electricity consumption.

CURRENT AND FUTURE DEVELOPMENTS

Recent advancements in renewable-energy-based cooling technologies have accelerated the development of sustainable air-conditioning systems with improved energy efficiency and reduced environmental impact. In solar-assisted cooling, considerable progress has been achieved in the design of high-efficiency evacuated tube and flat-plate solar collectors, advanced thermal energy storage systems, and intelligent control strategies that improve solar energy utilization and reduce auxiliary energy consumption. Similarly, significant developments in thermoelectric technology, including high-performance thermoelectric materials, nanostructured semiconductors, optimized module geometries, and advanced heat exchanger designs, have contributed to improving the cooling capacity and COP of thermoelectric air-conditioning systems. Furthermore, numerical simulation tools such as TRNSYS, EES, and computational optimization techniques have enabled more accurate prediction and optimization of system performance under varying climatic and operating conditions.

The present study contributes to these developments by integrating technical performance analysis, experimental validation, mathematical modeling, and economic optimization into a unified framework. The proposed ETCC criterion provides a practical approach for simultaneously evaluating cooling performance, investment cost, and operating cost, thereby supporting the optimal design of

© STM Journals 2026. All Rights Reserved

environmentally friendly residential air-conditioning systems. The comparative evaluation of water-cooled and air-cooled LiBr–H_2O absorption chillers, together with the optimization of thermoelectric module configuration, collector area, thermal storage capacity, and operating current, offers useful design guidelines for future renewable cooling applications.

Future research should focus on the experimental implementation and long-term field validation of integrated solar-assisted and thermoelectric cooling systems under different climatic conditions. The incorporation of next-generation thermoelectric materials with higher figures of merit (ZT), phase-change thermal energy storage, advanced heat exchangers, and hybrid photovoltaic–thermal (PVT) systems could further improve the overall system efficiency. In addition, artificial intelligence (AI)-based predictive control, machine learning algorithms, digital twin technologies, and Internet of Things (IoT)-enabled monitoring systems may be employed to optimize real-time system operation and energy management. Future studies should also include dynamic performance analysis, life cycle assessment, environmental impact evaluation, uncertainty analysis, and multi-objective optimization considering energy efficiency, economic feasibility, carbon emission reduction, and occupant thermal comfort. These developments will facilitate the commercialization and wider adoption of sustainable, energy-efficient, and economically viable air-conditioning systems for residential and commercial buildings while supporting global decarbonization and net-zero energy targets.

REFERENCES

1. Mao N, Pan D, Li Z, Xu Y, Song M, Deng S. A numerical study on influences of building envelope heat gain on operating performances of a bed-based task/ambient air conditioning (TAC) system in energy saving and thermal comfort. Appl Energy. 2017;192:213-21. doi:10.1016/j.apenergy.2017.02.027.
2. Mei J, Xia X. Energy-efficient predictive control of indoor thermal comfort and air quality in a direct expansion air conditioning system. Appl Energy. 2017;195:439-52. doi:10.1016/j.apenergy.2017.03.076.
3. Randazzo T, De Cian E, Mistry MN. Air conditioning and electricity expenditure: the role of climate in temperate countries. Econ Model. 2020;90:273-87. doi:10.1016/j.econmod.2020.05.001.
4. Davis LW, Gertler PJ. Contribution of air conditioning adoption to future energy use under global warming. Proc Natl Acad Sci U S A. 2015;112(19):5962-7. doi:10.1073/pnas.1423558112.
5. Lickley M, Solomon S, Fletcher S, Velders GJM, Daniel J, Rigby M, et al. Quantifying contributions of chlorofluorocarbon banks to emissions and impacts on the ozone layer and climate. Nat Commun. 2020;11(1):1380. doi:10.1038/s41467-020-15162-7.
6. Hurwitz MM, Fleming EL, Newman PA, Li F, Mlawer E, Cady-Pereira K, et al. Ozone depletion by hydrofluorocarbons. Geophys Res Lett. 2015;42:8686-92. doi:10.1002/2015GL065856.
7. Nishimwe AMR, Reiter S. Estimation, analysis and mapping of electricity consumption of a regional building stock in a temperate climate in Europe. Energy Build. 2021;253:111535. doi:10.1016/j.enbuild.2021.111535.
8. United Nations Environment Programme. HFCs: A Critical Link in Protecting Climate and the Ozone Layer. Nairobi: United Nations Environment Programme; 2011.
9. Lim DK, Ahn BH, Jeong JH. Method to control an air conditioner by directly measuring the relative humidity of indoor air to improve the comfort and energy efficiency. Appl Energy. 2018;215:290-9. doi:10.1016/j.apenergy.2018.02.004.
10. Mei J, Xia X, Song M. An autonomous hierarchical control for improving indoor comfort and energy efficiency of a direct expansion air conditioning system. Appl Energy. 2018;221:450-63. doi:10.1016/j.apenergy.2018.03.162.
11. Liu ZB, Zhang L, Gong GC, Luo YQ, Meng FF. Experimental study and performance analysis of a solar thermoelectric air conditioner with hot water supply. Energy Build. 2015;86:619-25. doi:10.1016/j.enbuild.2014.10.053.
12. Liu ZB, Zhang L, Gong GC. Experimental evaluation of a solar thermoelectric cooled ceiling combined with displacement ventilation system. Energy Convers Manag. 2014;87:559-65. doi:10.1016/j.enconman.2014.07.051.

© STM Journals 2026. All Rights Reserved

13. Dongxu J, Zhongbao W, Pou J, Mazzoni S, Rajoo S, Romagnoli A. Geometry optimization of thermoelectric modules: simulation and experimental study. Energy Convers Manag. 2019;195:236-43. doi:10.1016/j.enconman.2019.05.003.
14. Attar A, Lee H. Designing and testing the optimum design of automotive air-to-air thermoelectric air conditioner (TEAC) system. Energy Convers Manag. 2016;112:328-36. doi:10.1016/j.enconman.2016.01.029.
15. Martinez A, Díaz de Garayo S, Aranguren P, Araiz M, Catalán L. Simulation of thermoelectric heat pumps in nearly zero energy buildings: why do all models seem to be right? Energy Convers Manag. 2021;235:113992. doi:10.1016/j.enconman.2021.113992.
16. Martinez A, Díaz de Garayo S, Aranguren P, Astrain D. Assessing the reliability of current simulation of thermoelectric heat pumps for nearly zero energy buildings: expected deviations and general guidelines. Energy Convers Manag. 2019;198:111834. doi:10.1016/j.enconman.2019.111834.
17. Provensi A, Barbosa JR. Analysis and optimization of air coolers using multiple-stage thermoelectric modules arranged in counter-current flow. Int J Refrig. 2020;110:19-27. doi:10.1016/j.ijrefrig.2019.10.014.
18. Oh MS, Ahn JH, Kim DW, Jang DS, Kim Y. Thermal comfort and energy saving in a vehicle compartment using a localized air-conditioning system. Appl Energy. 2014;133:14-21. doi:10.1016/j.apenergy.2014.07.089.
19. Ruiz-Ortega PE, Olivares-Robles MA, Badillo-Ruiz CA. Transient thermal behavior of a segmented thermoelectric cooler with variable cross-sectional areas. Int J Energy Res. 2021;45:19215-25. doi:10.1002/er.7123.
20. Yilmazoglu MZ. Experimental and numerical investigation of a prototype thermoelectric heating and cooling unit. Energy Build. 2016;113:51-60. doi:10.1016/j.enbuild.2015.12.046.
21. Shittu S, Li G, Zhao X, Ma X. Review of thermoelectric geometry and structure optimization for performance enhancement. Appl Energy. 2020;268:115075. doi:10.1016/j.apenergy.2020.115075.
22. Fabián-Mijangos A, Min G, Alvarez-Quintana J. Enhanced performance thermoelectric module having asymmetrical legs. Energy Convers Manag. 2017;148:1372-81. doi:10.1016/j.enconman.2017.06.087.
23. Wang X, Qi JI, Deng W, Li G, Gao X, He L, et al. An optimized design approach concerning thermoelectric generators with frustum-shaped legs based on three-dimensional multiphysics model. Energy. 2021;233:120810. doi:10.1016/j.energy.2021.120810.
24. Tian XX, Asaadi S, Moria H, Kaood A, Pourhedayat S, Jermsittiparsert K. Proposing tube-bundle arrangement of tubular thermoelectric module as a novel air cooler. Energy. 2020;208:118428. doi:10.1016/j.energy.2020.118428.
25. Sun H, Lin B, Lin Z, Zhu Y, Li H, Wu X. Research on a radiant heating terminal integrated with a thermoelectric unit and flat heat pipe. Energy Build. 2018;172:209-20. doi:10.1016/j.enbuild.2018.04.054.
26. Conrad KJ. A physics-based compact model for thermoelectric devices [thesis]. West Lafayette (IN): Purdue University; 2015. Available from: https://docs.lib.purdue.edu/open_access_theses/539.
27. Pourkiaei SM, Ahmadi MH, Sadeghzadeh M, Moosavi S, Pourfayaz F, Chen L, et al. Thermoelectric cooler and thermoelectric generator devices: a review of present and potential applications, modeling and materials. Energy. 2019;186:115849. doi:10.1016/j.energy.2019.07.179.
28. Eivari HA, Sohbatzadeh Z, Mele P, Assadi MHN. Low thermal conductivity: fundamentals and theoretical aspects in thermoelectric applications. Mater Today Energy. 2021;21:100744. doi:10.1016/j.mtener.2021.100744.
29. Luo D, Wang R, Yu W, Zhou W. Performance optimization of a converging thermoelectric generator system via multiphysics simulations. Energy. 2020;204:117974. doi:10.1016/j.energy.2020.117974.
30. Junior C, Richter C, Tegethoff W, Lemke N, Köhler J. Modeling and simulation of a thermoelectric heat exchanger using the object-oriented library TIL. Proceedings of the 6th International Modelica Conference; 2008 Mar 3–4. Modelica Association; 2008. p. 437–45.

© STM Journals 2026. All Rights Reserved

31. Selvam C, Manikandan S, Krishna NV, Lamba R, Kaushik SC, Mahian O. Enhanced thermal performance of a thermoelectric generator with phase change materials. Int Commun Heat Mass Transf. 2020;114:104561. doi:10.1016/j.icheatmasstransfer.2020.104561.
32. Tang R, Wang S, Shan K, Cheung H. Optimal control strategy of central air-conditioning systems of buildings at morning start period for enhanced energy efficiency and peak demand limiting. Energy. 2018;151:771-81. doi:10.1016/j.energy.2018.03.032.
33. Beghi A, Cecchinato L, Rampazzo M. A multi-phase genetic algorithm for the efficient management of multi-chiller systems. Energy Convers Manag. 2011;52(3):1650-61. doi:10.1016/j.enconman.2010.10.028.
34. Jia J, Lee WL, Cheng Y, Tian QI. Can reversible room air-conditioner be used for combined space and domestic hot water heating in subtropical dwellings? Techno-economic evidence from Hong Kong. Energy. 2021;223:119911. doi:10.1016/j.energy.2021.119911.
35. Niemann P, Schmitz G. Air conditioning system with enthalpy recovery for space heating and air humidification: an experimental and numerical investigation. Energy. 2020;213:118789. doi:10.1016/j.energy.2020.118789.
36. Luqman M, Al-Ansari T. A novel integrated wastewater recovery, clean water production and air-conditioning system. Energy Convers Manag. 2021;244:114525. doi:10.1016/j.enconman.2021.114525.
37. Multicomp Pro. Thermoelectric module MCTE1-19913L-S [datasheet on the Internet]. Farnell; 2023. Available from: https://www.farnell.com/datasheets/3986568.pdf
38. Buchalik R, Nowak G, Nowak I. Mathematical model of a thermoelectric system based on steady- and rapid-state measurements. Appl Energy. 2021;293:116943. doi:10.1016/j.apenergy.2021.116943.
39. Li W, Paul MC, Montecucco A, Siviter J, Knox AR, Sweet T, et al. Multiphysics simulations of thermoelectric generator modules with cold and hot blocks and effects of some factors. Case Stud Therm Eng. 2017;10:63-72. doi:10.1016/j.csite.2017.03.005.
40. Desideri U, Proietti S, Sdringola P. Solar-powered cooling systems: technical and economic analysis on industrial refrigeration and air-conditioning applications. Appl Energy. 2009;86(9):1376-86. doi:10.1016/j.apenergy.2009.01.011.
41. Eicker U, Pietruschka D. Design and performance of solar powered absorption cooling systems in office buildings. Energy Build. 2009;41(1):81-91. doi:10.1016/j.enbuild.2008.07.015.
42. Henning HM. Solar assisted air conditioning of buildings—an overview. Appl Therm Eng. 2007;27(10):1734-49. doi:10.1016/j.applthermaleng.2006.07.021.
43. Klein SA, Duffie JA, Mitchell JC, Kummer JP, Bechkman WA, Duffie NA, et al. TRNSYS: a transient simulation program user's manual. Madison (WI): University of Wisconsin-Madison; 1994.
44. F-Chart Software. Engineering Equation Solver (EES): User's Manual and Program Documentation. Middleton (WI): F-Chart Software; 2008.
45. Bakhtiari B, Fradette L, Legros R, Paris J. A model for analysis and design of H_2O-LiBr absorption heat pumps. Energy Convers Manag. 2011;52(2):1439-48. doi:10.1016/j.enconman.2010.09.037.
46. Castaing-Lasvignottes J. Aspects thermodynamiques et technico-économiques des systèmes à absorption liquide [Online]. 2001. Available from: http://jc.castaing.free.fr/ens/abs/abscours.pdf
47. Kim DS, Infante Ferreira CA. Air-cooled LiBr–water absorption chillers for solar air conditioning in extremely hot weathers. Energy Convers Manag. 2009;50(4):1018-25. doi:10.1016/j.enconman.2008.12.021.
48. Banque Centrale de Tunisie. Monetary policy and exchange rate [Online]. Tunis: Banque Centrale de Tunisie; 2011. Available from: https://www.bct.gov.tn/bct/siteprod/francais/politique/index_suite.jsp
49. Li X, Wu W, Zhang X, Shi W, Wang B. Energy saving potential of low temperature hot water system based on air source absorption heat pump. Appl Therm Eng. 2012;48:317-24. doi:10.1016/j.applthermaleng.2011.12.045.
50. Mahjouri F, Nunez A. The relative cost of solar thermal collector installations [Online]. 2010. Available from: https://www.yumpu.com/en/document/view/36689557/the-relative-cost-of-solar-thermal-collector-installation

© STM Journals 2026. All Rights Reserved

51. Mateus T, Oliveira AC. Energy and economic analysis of an integrated solar absorption cooling and heating system in different building types and climates. Appl Energy. 2009;86:949-57. doi:10.1016/j.apenergy.2008.09.005.
52. Kim DS, Infante Ferreira CA. Solar refrigeration options: a state-of-the-art review. Int J Refrig. 2008;31(1):3-15. doi:10.1016/j.ijrefrig.2007.07.011.
53. Wang K, Abdelaziz O, Kisari P, Vineyard EA. State-of-the-art review on crystallization control technologies for water/LiBr absorption heat pumps. Int J Refrig. 2011;34(6):1325-37. doi:10.1016/j.ijrefrig.2011.04.006.
54. Tippayawong N, Chaichana C, Promwangkwa A, Rerkkriangkrai P. Gasification of cashew nut shells for thermal application in local food processing factory. Energy Sustain Dev. 2011;15:69-72. doi:10.1016/j.esd.2010.10.001.
55. Zogg RA, Feng MY, Westphalen D. Guide to developing air-cooled LiBr absorption for combined heat and power applications [report]. United States Department of Energy; 2005.
56. Wei Q, Qu Y, Tan T. Mass and heat balance calculations and economic evaluation of an innovative biomass pyrolysis project. Front Chem Sci Eng. 2011;5(3):355-61. doi:10.1007/s11705-010-0567-9.
57. Tippayawong N, Chaichana C, Promwungkwa A, Rerkkriangkrai P. Investigation of a small biomass gasifier–engine system operation and its application to water pumping in rural Thailand. Energy Sources A Recovery Util Environ Eff. 2013;35:476-86. doi:10.1080/15567036.2010.511433.
58. Wongsiriamnuay T, Tippayawong N. Product gas distribution and composition from catalyzed gasification of Mimosa. Int J Renew Energy Res. 2012;2(3):363-8. Available from: https://izlik.org/JA26KT34RT
59. Wongsiriamnuay T, Kannang N, Tippayawong N. Effect of operating conditions on catalytic gasification of bamboo in a fluidized bed. Int J Chem Eng. 2013;2013:297941. doi:10.1155/2013/297941.
60. Khongkrapan P, Thanompongchart P, Tippayawong N, Kiatsiriroat T. Microwave plasma assisted pyrolysis of refuse derived fuels. Open Eng. 2014;4:72-9. doi:10.2478/s13531-013-0142-5.
61. Sittisun P, Tippayawong N, Wattanasiriwech D. Thermal degradation characteristics and kinetics of oxy combustion of corn residues. Adv Mater Sci Eng. 2015;2015:304395. doi:10.1155/2015/304395.
62. Chaiwong K, Kiatsiriroat T, Vorayos N, Thararax C. Biochar production from freshwater algae by slow pyrolysis. Maejo Int J Sci Technol. 2012;6:186-95.
63. Chaiwong K, Kiatsiriroat T, Vorayos N, Thararax C. Study of bio-oil and bio-char production from algae by slow pyrolysis. Biomass Bioenergy. 2013;56:600-6. doi:10.1016/j.biombioe.2013.05.035.
64. Ringer M, Putsche V, Scahill J. Large-scale pyrolysis oil production: a technology assessment and economic analysis [technical report]. Report No. NREL/TP-510-37779. National Renewable Energy Laboratory; 2006.
65. Mei F, Dudukovic M, Evans M, Carpenter N. Mass and energy balance for a corn-to-ethanol plant [master's thesis]. St. Louis (MO): Washington University in St. Louis; 2005.
66. Crombie K, Mašek O. Investigating the potential for a self-sustaining slow pyrolysis system under varying operating conditions. Bioresour Technol. 2014;162:148-56. doi:10.1016/j.biortech.2014.03.134.
67. Sinha S, Jhalani A, Ravi MR, Ray A. Modelling of pyrolysis in wood: a review. J Sol Energy Soc India. 2000;10:41-62.
68. Boateng AA, Mullen CA, Osgood-Jacobs L, Carlson P, Macken N. Mass balance, energy, and exergy analysis of bio-oil production by fast pyrolysis. J Energy Resour Technol. 2012;134:042001. doi:10.1115/1.4007659.
69. Cottam ML, Bridgwater AV. Techno-economic modelling of biomass flash pyrolysis and upgrading systems. Biomass Bioenergy. 1994;7:267-73. doi:10.1016/0961-9534(94)00068-5.
70. Gregoire CE, Bain RL. Technoeconomic analysis of the production of biocrude from wood. Biomass Bioenergy. 1994;7:275-83. doi:10.1016/0961-9534(94)00069-6.
71. Garcia-Nunez JA, Pelaez-Samaniego MR, Garcia-Perez ME, Fonts I, Abrego J, Westerhof RJM, et al. Historical developments of pyrolysis reactors: a review. Energy Fuels. 2017;31:5751-75. doi:10.1021/acs.energyfuels.7b00641.

© STM Journals 2026. All Rights Reserved

72. Mkhize NM, Danon B, Alvarez J, Lopez G, Amutio M, Bilbao J, et al. Influence of reactor and condensation system design on tyre pyrolysis products yields. J Anal Appl Pyrolysis. 2019;143:104683. doi:10.1016/j.jaap.2019.104683.
73. Talwar P, Agudelo MA, Nanda S. Pyrolysis process, reactors, products, and applications: a review. Energies. 2025;18:2979. doi:10.3390/en18112979.
74. Karvonen J, Kunttu J, Suominen T, Kangas J, Leskinen P, Judl J. Integrating fast pyrolysis reactor with combined heat and power plant improves environmental and energy efficiency in bio-oil production. J Clean Prod. 2018;183:143-52. doi:10.1016/j.jclepro.2018.02.143.
75. Comendador P, Santamaria L, Amutio M, Alvarez J, Olazar M, Lopez G. Energy analysis and heat integration in the joint process of biomass fast pyrolysis and in-line sorption-enhanced steam reforming. Energy Fuels. 2024;38:14402-13. doi:10.1021/acs.energyfuels.4c02555.
76. Yang Y, Brammer JG, Wright DG, Scott JA, Serrano C, Bridgwater AV. Combined heat and power from the intermediate pyrolysis of biomass materials: performance, economics and environmental impact. Appl Energy. 2017;191:639-52. doi:10.1016/j.apenergy.2017.02.004.
77. Crombie K, Mašek O. Investigating the potential for a self-sustaining slow pyrolysis system under varying operating conditions. Bioresour Technol. 2014;162:148-56. doi:10.1016/j.biortech.2014.03.134.
78. Ábrego J, Atienza-Martínez M, Plou F, Arauzo J. Heat requirement for fixed bed pyrolysis of beechwood chips. Energy. 2019;178:145-57. doi:10.1016/j.energy.2019.04.078.

© STM Journals 2026. All Rights Reserved